Model for low-energy electronic states probed by x-ray absorption in high-T_c cuprates

Mark S. Hybertsen
AT&T Bell Laboratories, 600 Mountain Avenue, Murray Hill, New Jersey 07974

E. B. Stechel
Condensed Matter Theory Division 1151, Sandia National Laboratories, Albuquerque, New Mexico 87185

W. M. C. Foulkes* and M. Schlüter
AT&T Bell Laboratories, 600 Mountain Avenue, Murray Hill, New Jersey 07974
(Received 4 November 1991)

The low-energy electronic states in $La_{2-x}Sr_xCuO_4$ have recently been probed by soft-x-ray-absorption measurements as a function of doping (x) from the insulating well into the metallic (superconducting) regime. A model for understanding and interpreting those spectra is presented. The electronic structure of the active Cu-O planes is represented by an extended three-band Hubbard model whose parameters have been previously derived from quantum-chemical calculations. The essential additional Coulomb interaction between the core hole created in the absorption process and the nearby valence electrons has been included by calculating the necessary on-site and nearest-neighbor core-valence Coulomb parameters. The absorption spectra are calculated using exact-diagonalization techniques for finite clusters. The low-energy electronic structure can be represented within an effective one-band Hubbard model whose parameters are obtained by a mapping from the three-band model. The transition operator for the absorption process as well as the core-hole Coulomb potential are also mapped into the one-band model. The final calculations in the one-band model are performed for the insulator (half filling) and for several excess hole concentrations in the metal. The theoretical and experimental spectra are compared in detail. The calculations accurately account for the observed peak intensities as a function of doping. Important features include the gap between the preedge peaks in the metal, core-hole excitonic effects, and transfer of oscillator strength. In particular, the preedge peak separation is the charge-transfer gap (from the insulator) reduced by the core-hole exciton binding energy. The transfer of oscillator strength between the observed peaks, which is a key signature of the correlated band situation, is analyzed in detail. A doped charge-transfer insulator model for the electronic structure of the cuprates explains the essential features of the x-ray-absorption data.

I. INTRODUCTION

Various high-energy spectroscopic probes of the cuprate materials continue to play an important role in understanding their underlying electronic structure. These include (inverse) photoemission spectroscopy,[1-7] electron-energy-loss spectroscopy (EELS),[8-13] and x-ray-absorption spectroscopy (XAS).[7,14-19] The picture emerging suggests that the insulating parent compounds fall in the class of charge-transfer insulators.[20] This emphasizes the importance of both the chemical character of the valence states (Cu d character and O p character) as well as the role of strong local Coulomb interactions, primarily in the Cu d channel.[1-4] A difficult current problem is to understand the systematic development of the low-energy electronic structure as the parent insulators are doped, taking the materials into the metallic (superconducting) regime. This problem has been controversial. Early on, XAS established the oxygen p character of the holelike carriers introduced upon doping.[7,8] This is consistent with the naive picture that hole doping pulls the Fermi level from the gap into the O ligand band as in a hole-doped semiconductor. However, photoemission data have been interpreted in terms of a collapse upon doping of the correlation-induced charge-transfer gap and the recovery of a more conventional (albeit interacting) bandlike picture.[6] Quite recent EELS (Ref. 12) and XAS (Ref. 19) data provide systematic, high-resolution spectra as a function of doping. It is the goal of the present work to provide a detailed understanding of these spectra and discuss the implications for a model of the electronic states near the Fermi level.

X-ray absorption involves transitions from occupied core levels (e.g., O 1s for spectra near the O K edge) into available empty states above the Fermi level. In the independent-particle (bandlike) picture, this simply probes the empty density of states, projected onto a particular local symmetry by a dipole selection rules (e.g., O p-like states). However, the interaction of the core hole created in this process with the valence electrons forms a classic many-body problem. The Mahan–Nozières–De Dominicis (MND) solution is well known for the case of free-electron-like metals (i.e., neglecting interactions among the valence electrons as well as band-structure effects).[21] The combination of excitonic effects[22] and the "orthogonality catastrophe"[23] yield the associated edge singularities in both absorption and emission spectra. The interaction of the valence electrons with a core hole

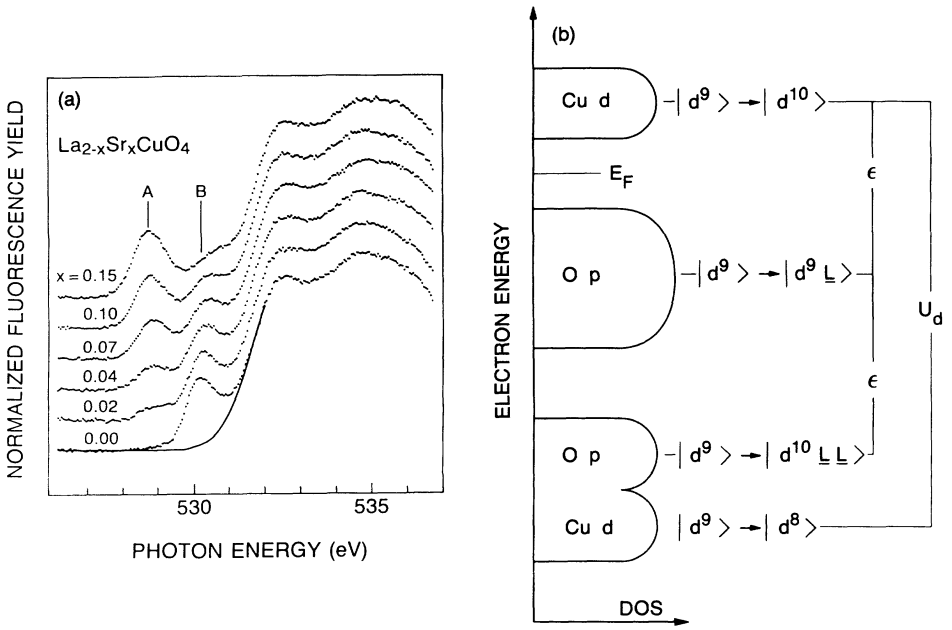

FIG. 1. (a) Normalized fluorescence yield at the O K edge of $La_{2-x}Sr_xCuO_{4+\delta}$. The solid curves are a common background. (Ref. 19). (b) A simplified view of the electronic structure of the CuO_2 planes showing the approximate local character of the transitions responsible for states above and below the Fermi level.

qualitatively alters the spectra. In considering the XAS for the cuprates, these effects must be included. However, the cuprates offer an additional challenge in that strong correlation effects are also essential to describe the valence electrons. The MND problem must be reanalyzed including these interactions.

The recent XAS results upon which we will focus are reproduced in Fig. 1(a). Experimental details may be found in Refs. 17 and 19 and references therein. The fluorescence detection method employed ensures that $\sim$2500 Å of materials is probed; consequently this is a bulk sensitive measurement. The key features are the following. For the insulating compound La_2CuO_4, the spectrum shows a single "preedge" peak (B) near 530 eV before the onset of the main O K edge. Upon doping with Sr, the $La_{2-x}Sr_xCuO_4$ samples yield spectra with an additional lower-energy peak (A) which grows in near 529 eV. The strong absorption above 531 eV is largely invariant with Sr doping being due to La d- and f-state wavefunction tails with p-like projection around the O sites. This will not further concern us here. Overall, the preedge peaks are separated by an energy (1.3 eV) comparable to, but smaller than, the optical threshold in La_2CuO_4 [$\approx$1.8 eV (Ref. 24)]. The intensity in the lower peak (A) grows systematically while that in the upper peak (B) decreases with doping. The intensity in peak B is nonetheless still quite evident for $x=0.15$, well into the metallic (superconducting) regime. There is also a systematic dispersion of the peaks with doping. The recent EELS data show qualitatively the same features.[12] Data for Li-doped NiO follows a similar pattern, including the decay of intensity in the upper peak.[25]

In Fig. 1(b), the charge-transfer picture[20] of the valence electronic structure is sketched. The picture is based on the observation that the insulating ground state is dominated by local Cu^{2+} ions in a $|d^9\rangle$ configuration. This accounts for the local $S=\frac{1}{2}$ moment observed in the magnetic insulators. Hybridization mixes in configurations with the hole in the O p band (ligand band, $|\underline{L}\rangle$). In practice, this is a strong effect, so Fig. 1(b) is oversimplified. Consider the insulator first. The electronic structure probed spectroscopically involves addition and/or removal of an electron. The dominant configurations involved in these transitions are identified and indicated as bands above and below the Fermi level corresponding to inverse photoemission (IPES) and photoemission (PES), respectively. The first available states for adding an electron involve filling a Cu d state locally. On the other hand, the lowest-energy transition for removing an electron creates a hole in the ligand band separated from the Cu d level by the chemically derived energy ε. The energy to remove an electron from the local Cu d state is substantially larger because of the sizable Coulomb repulsion between the two Cu d holes, U_d, in the final state. The XAS probes the empty states as in IPES, but with local chemical specificity, e.g., the ligand components. In the insulator, the empty band is accessible due to the hybridization. Now, the naive view of hole doping involves pulling the Fermi level into the ligand band. Then new states become available, separated by a gap from the states already probed in the insulator. The data in Fig. 1(a) are qualitatively consistent with this

simplified picture of a doped charge-transfer insulator. However, the loss of strength in the upper peak (B) is a characteristic feature of the data, which requires a more detailed understanding.

The essential features of the valence electronic structure, including Coulomb correlations, are described initially by a three-band Hubbard model involving the Cu $d(x^2-y^2)$ and corresponding in-plane $p\sigma(x,y)$ orbitals.[26] This allows an accurate representation of both the Cu d and O p degrees of freedom which enter the present problem. The Cu $d(3z^2-r^2)$and other ligand orbitals are neglected. This is justified in part experimentally by the small z component observed in polarized EELS (Refs. 10, 11, and 13) and XAS (Ref. 14) measurements[27] and in part theoretically on the basis of band-structure calculations.[28,29] The parameters for the model were derived earlier from quantum-chemical calculations.[28] In order to handle the MND problem, including the valence correlations, exact diagonalization techniques are applied to finite clusters. This has the advantage of treating all the correlations exactly, but only for very small clusters. The cluster-size limitation is alleviated to some extent by mapping the electronic structure[30] and the x-ray-absorption process into an effective one-band Hubbard model. This mapping can be done accurately for the empty band together with the band introduced by doping and allows for sufficiently large clusters to be treated.

A full analysis of the O K-edge XAS is given as a function of doping. A brief account was presented in Ref. 19. Quantitative comparison is made to the experimental spectra. The favorable agreement supports the present Hubbard model for the electronic structure. The combination of the experiment data with the present theory contradicts models where the correlation gap collapses. However, the naive picture of doping is not fully correct either. Such thinking, based on an ionic, independent-particle model for the insulating gap, does not capture the transfer of oscillator strength observed with doping. We show in detail that it occurs, however, naturally within the Hubbard model. This transfer is a characteristic feature of the correlated band picture. It is this support for the correlated band picture (present Hubbard model or extensions of it) that is the central result of the present work.

The balance of the paper is organized as follows. The three-band Hubbard model used to describe the valence-band electronic structure is summarized in Sec. II. The valence-core Coulomb interactions are obtained and the model for the XAS is given. In Sec. III, the mapping to the one-band Hubbard model is given and tested. The method for treating the doped materials is presented. The results for the XAS appear in Sec. IV and these are compared to experiment. The role of core-hole excitonic effects is discussed. The characteristic transfer of oscillator strength is analyzed in Sec. V. In Sec. VI, the present results are briefly compared with some other probes of states near the Fermi level. Concluding remarks appear in Sec. VII. An appendix analyzes the effect of strong impurity potentials on the XAS.

By convention, all operators are in the hole picture. Hole creation physically refers to photoemission probing states spectroscopically below the Fermi level and hole annihilation probes states above the Fermi level. However, for clarity, all spectra are presented and discussed in the standard electron picture, i.e., with PES below the Fermi level at low energy and IPES (XAS) spectra above the Fermi level at higher energy.

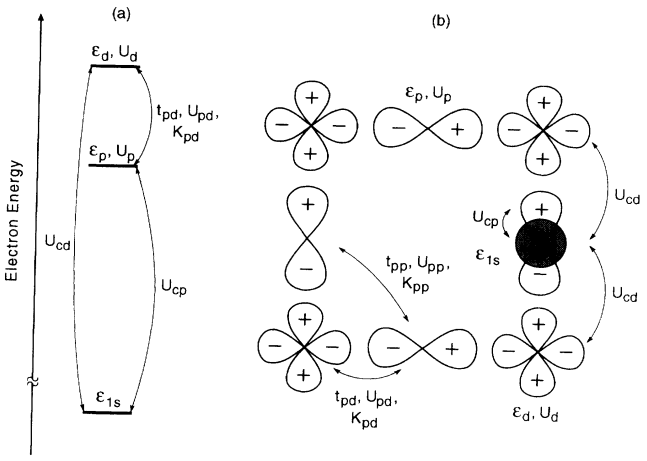

FIG. 2. Illustration of the extended three-band Hubbard model showing all the interactions including those involving the O 1s core level. (a) The level structure shown for electron energies. (b) The orbitals retained in the CuO_2 planes.

II. X-RAY-ABSORPTION IN A THREE-BAND HUBBARD MODEL

A. Three-band Hubbard model

Early on, it was suggested that a three-band Hubbard model is an appropriate starting point for the electronic structure of CuO_2 planes common to all superconducting cuprates.[26] The self-consistent band-structure calculations showed that the bands near the Fermi level are dominated by the Cu $d(x^2-y^2)$ orbital strongly hybridized with the associated O $p\sigma(x,y)$ orbitals.[29] These are the orbitals which are explicitly treated in the three-band Hubbard model with the assumption that no other orbitals directly enter into the low-energy dynamics. The other orbitals do renormalize (screen) the parameters which describe the orbitals explicitly retained. In formal terms, the CuO_2 planes consist of Cu^{2+} and O^{2-} ions for the insulating parent materials. Therefore it is natural to adopt a hole picture to describe the Hamiltonian. The vacuum configuration is taken to be $|d^{10}p^6\rangle$ so the ground state consists of one hole per formula unit.

The parameters which are included in the model are illustrated in Fig. 2. These fall into three categories: one electron on-site and hopping integrals, direct Coulomb integrals, and exchange Coulomb integrals. The Hamiltonian is truncated after two neighbor shells:[31]

$$H_{\rm val}=\sum_{\sigma}\Big[\varepsilon_d n_{d\sigma}\varepsilon_p n_{p\sigma}+(t_{pd}c^{\dagger}_{p\sigma}c_{d\sigma}+t_{pp'}c^{\dagger}_{p\sigma}c_{p'\sigma}+\text{H.c.})+\tfrac{1}{2}U_d n_{d\sigma}n_{d-\sigma}+\tfrac{1}{2}U_p n_{p\sigma}n_{p-\sigma}$$
$$+\sum_{\sigma'}(U_{pd}n_{p\sigma}n_{d\sigma'}+U_{pp'}n_{p\sigma}n_{p'\sigma'}+K_{pd}c^{\dagger}_{p\sigma}c_{p\sigma}c^{\dagger}_{d\sigma'}c_{d\sigma}+K_{pp'}c^{\dagger}_{p\sigma}c_{p\sigma}c^{\dagger}_{p'\sigma'}c_{p'\sigma})\Big] . \quad (1)$$

Here the hole creation operators $c^{\dagger}_{d\sigma}$ and $c^{\dagger}_{p\sigma}$ act on the Cu $d(x^2-y^2)$ and O $p\sigma(x,y)$ channels, respectively, with density operators, e.g., $n_{p\sigma}=c^{\dagger}_{p\sigma}c_{p\sigma}$. The explicit lattice site indices have been suppressed for clarity.

The parameters for the three-band Hubbard model appropriate for the cuprates have been discussed by several groups based on first-principles calculations,[28,32,33] detailed analysis of experiment[34,35] and general arguments.[31] There is general agreement on the values. We use the values we obtained previously[28,30] for La_2CuO_4 (Table I). The resulting model Hamiltonian has been studied extensively using exact diagonalization techniques for small clusters. From studies with the present (or similar) parameters for the cuprates, it has been found that this model accurately represents various properties of the cuprates when compared to experiment. The insulator is found to be accurately represented by an $S=\frac{1}{2}$ Heisenberg antiferromagnet with the superexchange of the correct magnitude.[30–32] The charge-transfer gap is approximately correct.[30,32,35] The position and resonance properties of the satellite features in the PES are correct.[35,36] Finally, the dynamics of carriers are found to be approximately symmetric between electrons and holes,[30] in agreement with the doping dependence of the low-frequency oscillator strength observed in optical measurements.[37]

In the presence work on the x-ray-absorption spectra, we use this parameter set without further adjustment.

B. X-ray-absorption process

The core hole created during the x-ray absorption is described by (Fig. 2)

$$H_{\rm core}=\varepsilon_{1s}n_{1s}+U_{cp}n_c n_{1s}+\sum_{\delta}U_{cd}n_{d\delta}n_{1s} , \quad (2)$$

where the sum over the O sites is implicit and δ refers to the neighboring Cu sites. This has been written for the case of an O 1*s* core hole. In accordance with the final-state picture, it is assumed that screening of the core hole is fast compared to the lifetime of the core hole as well as the time scale for the absorption process. Therefore the parameters in Eq. (2) are assumed to be statically screened. The exchange terms in the core-valence Coulomb interaction are neglected.

The dipole selection rule appropriate to the absorption process is assumed to limit the final-state electron to the same site as the core hole. The value of the dipole matrix element is absorbed into an overall constant. The absorption cross section is

$$A(\omega)=B\sum_{n,\sigma}|\langle N,n|c^{\dagger}_{1s\sigma}c_{p\sigma}|N,0\rangle|^2$$
$$\times F(\hbar\omega-(E_{N,n}-E_{N,0})) . \quad (3)$$

In this expression, the state vectors are full many-body eigenstates with N holes including a core hole in the final state and n indexes the final states. The usual δ function has been replaced by a general line-shape function to account for the finite lifetime of the core hole, phonon dynamics, and instrumental resolution. For systems with translation symmetry, Eq. (3) gives the absorption per O site. If there are other perturbations, e.g., impurity potentials, then the spectra must be averaged over distinct O sites. No fluctuations in the core-hole number are being considered explicitly. Then the evaluation of Eq. (3) is similar to the one-particle Green's function appropriate for IPES, but where the Hamiltonian for the final states includes the potential due to the core hole.

The calculations can be carried out for a finite number of particles and sites using direct diagonalization techniques.[38] For the line-shape function, a Gaussian is assumed. This is based on the resolution function for the experiments reported in Fig. 1(a) (0.3 eV Gaussian), the estimated contribution of phonon broadening (0.3 eV Gaussian), and the smaller contribution due to the O 1*s* inverse lifetime (0.2 eV Lorentzian for free atoms).[19] This leads to the final broadening employed: 0.5 eV Gaussian, full width at half maximum (FWHM). The 1*s* lifetime is likely to be shorter for O atoms in the solid due to increased *p*-shell occupancy[39] as well as intersite Auger processes.

The expression for the x-ray-absorption cross section includes all the elements of the classic MND problem. The excitonic interactions are present through the final-state Hamiltonian. The "orthogonality catastrophe" enters through the full many-body final-state wave function. In practice, the calculation is carried out for a finite (small) number of valence holes. Therefore, the final density of states and the edge singularities of the extended

TABLE I. Parameters for the three-band Hubbard model describing La_2CuO_4. Hole notation is used in connection with the phase conventions shown in Fig. 2.

U_d	U_p	U_{pd}	$U_{pp'}$	U_{cp}	U_{cd}	K_{pd}	$K_{pp'}$	$\varepsilon_p-\varepsilon_d$	t_{pd}	t_{pp}
10.5	4	1.2	0	6	1.2	−0.18	−0.04	3.6	1.3	0.65

system cannot be reproduced. However, given the amount of broadening described above, such long-time (asymptotic) behavior cannot be resolved experimentally either. The influence of finite-size effects can be checked computationally by comparing results from different size clusters.

C. Screened core-hole Coulomb interaction parameters

The procedure for calculating the necessary core-valence interaction parameters follows closely the earlier work of Ref. 28. The response of the valence electrons is calculated self-consistently in the presence of a frozen-core hole, e.g., an O 1*s* hole. The extra (screening) electron required to maintain charge neutrality is placed self-consistently into the valence bands. This procedure closely follows the conditions of the x-ray-absorption process so the screening response well represents the spectroscopy of interest. The core hole is introduced in a supercell geometry to isolate the local perturbations. For the present case, $\sqrt{2}\times\sqrt{2}$ and 2×2 unit cells were considered in the basal plane of La_2CuO_4 centered on an O site. The smaller cell was already adequate to represent the local response to the core hole. The calculations were carried out within the local-density approximation (LDA) of density-functional theory using the linearized-muffin-tin-orbital (LMTO) method.[40] The technical details are the same as described in Ref. 28, except the *f* orbitals on the La sites were dropped.

The dominant effect of the core hole is to strongly localize O 2*p* states on the same site. Figure 3 shows the local levels pulled out from the bottom of the bands. The two strong peaks correspond, respectively, to the $p\sigma$ orbital pointed towards the neighboring Cu sites and the two $p\pi$ orbitals which are orthogonal. The bound states reflect a strong 2*p* valence electron to 1*s* core-hole attraction, U_{cp} in Eq. (2). The nearest-neighbor U_{cd} results in a shift of Cu 3*d* states to lower energy on average, but no bound states are created.

In order to obtain the Coulomb interaction parameters, the effective local on-site energy is extracted from the LDA calculations. For the O 2*p* case, the lower of the bound peak positions is used, relative to the Fermi level. For the Cu 3*d* case, the shift in the average *d* energy is calculated by integrating over the Cu *d* density of states. In the context of the three-band model, treated within a mean-field approximation, these represent screened energies:[28]

$$\varepsilon_{d\sigma}^{\mathrm{MF}}=\varepsilon_d+U_{cd}+U_d\langle n_{d-\sigma}\rangle+4U_{pd}\langle n_p\rangle\ , \tag{4a}$$

$$\varepsilon_{p\sigma}^{\mathrm{MF}}=\varepsilon_p+U_{cp}+U_p\langle n_{p-\sigma}\rangle+2U_{pd}\langle n_d\rangle\ , \tag{4b}$$

where the densities are calculated in the presence of the core hole. The corresponding expression in the absence of a core hole (superscript 0) is used to obtain

$$(\varepsilon_d^{\mathrm{MF}}-\varepsilon_F)-(\varepsilon_d^{\mathrm{MF}}-\varepsilon_F)^0 = U_{cd}+\tfrac{1}{2}U_d(\langle n_d\rangle-\langle n_d\rangle^0)+U_{pd}(\langle n_p\rangle-\langle n_p\rangle^0)\ , \tag{5a}$$

$$(\varepsilon_p^{\mathrm{MF}}-\varepsilon_F)-(\varepsilon_p^{\mathrm{MF}}-\varepsilon_F)^0 = U_{cp}+\tfrac{1}{2}U_p(\langle n_p\rangle-\langle n_p\rangle^0)+2U_{pd}(\langle n_d\rangle-\langle n_d\rangle^0)\ . \tag{5b}$$

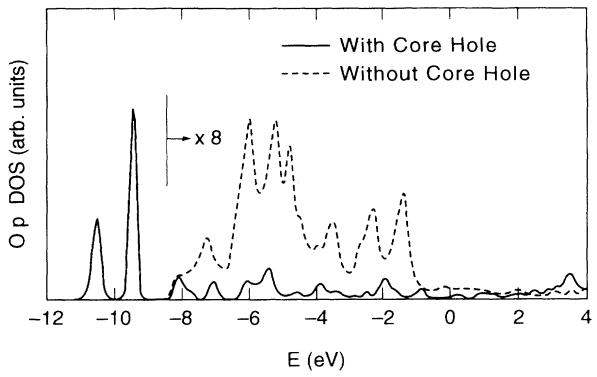

FIG. 3. In-plane oxygen *p*-like density of states with and without a frozen 1*s* O core-hole calculated within the LDA.

A paramagnetic solution has been imposed, consistent with the LDA calculations so the spin index has been suppressed. The zero superscript refers to unperturbed results. The numerical factors reflect the fact that only one O neighbor to the Cu is perturbed by the core hole while two Cu neighbors to the O are perturbed. Based on analysis of the LMTO results, the perturbation of the charge density beyond nearest neighbor is negligible. This expresses the needed Coulomb parameters in terms of changes induced by the core hole. The on-site energies are being compared relative to a Fermi level which would be unchanged in the limit of a large supercell.

The charge densities and energy shifts from the LMTO calculation have been analyzed to provide all the quantities needed in Eqs. (5) giving $U_{cp}=6\pm1$ eV and $U_{cd}=1.3\pm0.5$ eV. These satisfy $U_{cp}>U_p$ ($=4$ eV) and $U_{cd}\geq U_{pd}$ ($=1.2$ eV) as one would expect. Given the relatively large uncertainties in U_{cd}, we have chosen to fix it to the limit set by the valence *pd* interaction: $U_{cd}=1.2$ eV. The changes in density used in Fig. (5) should more properly have been calculated within the self-consistent mean-field treatment of the three-band model Eq. (1), rather than the full LMTO scheme. As a check, this mean-field calculation has been carried out with the present values of U_{cd} and U_{cp}; the resulting local levels agree with the LMTO calculations to within the overall error bars.

D. Comparison to band models

Recently, detailed LDA band calculations have been done for the O *K*-edge absorption cross section in CuO (Ref. 41) and $YBa_2Cu_3O_7$.[42] In both cases, an independent-particle model is applied so that the empty O 2*p* density of states, possibly weighted by dipole matrix elements, is compared to the measured spectrum. The advantage of the band approach is to include the microscopic chemical details of all the atomic states in the problem allowing the spectrum to be calculated over an energy range up to 20 eV above threshold. In Ref. 42, all the symmetry distinct O sites are considered, including the calculated chemical shifts. The results show that the features observed well above threshold are well explained

by the bandlike p-symmetry phase shifts. However, the region near threshold is not well represented. In particular, the details of the preedge peaks do not follow from the band model. For the case of CuO, a metallic band structure is used to model an antiferromagnetic insulator. The case of $YBa_2Cu_3O_7$ is more subtle. The presence of the chain states complicates the XAS.[42] This material is already metallic: the band theory and the photoemission agree in general terms with regards to band dispersions and Fermi surface.[43] Therefore band theory may appear to be adequate for this case.

The band model is deficient in several respects. First, the core-hole excitonic interactions have been neglected. Analysis of our results above the Fermi level shows that the inclusion of the core-hole potential significantly alters the state distribution near threshold but does not explain the observed spectra in Fig. 1(a). Second, the many-body matrix element for the absorption process is not considered. This has an important contribution to the line shape near threshold.[21–23] Finally, the band theory neglects essential correlations required to yield a gap in the insulating state. This is particularly important for understanding the evolution in the spectra of Fig. 1(a) from the insulating to the metallic state. In the band model, doping is represented by a right-band picture. As recognized in Ref. 42, this implies that the band model will not yield new features near threshold for the physically relevant range of doping.

III. X-RAY-ABSORPTION IN AN EFFECTIVE ONE-BAND HUBBARD MODEL

A. Effective one-band Hubbard model

The charge-transfer picture illustrated in Fig. 1(b) explicitly includes the chemically distinct Cu and O degrees of freedom. For a spectroscopy which covers the full valence band, this is essential. However, the dynamics of carriers near the charge-transfer gap region (or the Fermi level) may be described accurately by a simpler, effective Hamiltonian. Anderson suggested that the one-band Hubbard model would describe the essential dynamics.[44] Zhang and Rice gave explicit arguments based on an analysis of the three-band Hubbard model showing extra carriers could be described by an effective single-band model.[45] The hole case is nontrivial. The basic idea is that the extra hole goes into the ligand band, as shown in Fig. 1(b). The Cu d to O p hopping stabilizes the singlet combination of the ligand hold with a hole already present on a Cu site over the triplet combination. This bound singlet is split off from the ligand band edge and propagates through the otherwise interacting spin background via an effective one-band Hamiltonian, the so-called t-J model. These ideas have prompted considerable effort to analyze the three-band Hubbard model for realistic parameters to ascertain the applicability of one-band models.[30,46–50] Because of the large covalency, the mapping to an effective reduced-band model is not automatic. Nonetheless, it has been found that one-band Hubbard and single-band t-J models in fact can accurately represent the carrier dynamics for the present range of parameters.

We consider both sides of the charge-transfer gap on an equal footing using a one-band Hubbard model:

$$H_{\text{eff}}=\sum_{i\sigma}\varepsilon_i n_{i\sigma}+\sum_{i\delta\sigma}t c_{i\sigma}^{\dagger}c_{i+\delta\sigma} + \sum_{i\delta'\sigma}t' c_{i\sigma}^{\dagger}c_{i+\delta'\sigma}+\tfrac{1}{2}\sum_{i\sigma}U n_{i\sigma}n_{i-\sigma}\ . \tag{6}$$

The index δ (δ') corresponds to the (next)- nearest-neighbor sites. With reference to Fig. 1(b), and in a hole representation, the lower Hubbard band corresponds to the electron side of the charge-transfer gap while the upper Hubbard band represents the excess holes in the ligand band. One must recognize that the underlying chemical content of one hole on a site is mostly Cu d-like (about 80%) while two holes on a site are roughly 50% Cu d and 50% surrounding O p character.[30] The site index in Eq. (6) refers to an effective site consisting of a central Cu atom and surrounding O orbitals. Implicitly these are formed in an orthogonal set on a simple square lattice. The t refers to nearest-neighbor hopping energy while t' refers to the second-neighbor hopping energy across the diagonal. The effective U is equivalent to the charge-transfer gap for a CuO_4 cluster.

The parameter values for Eq. (6) as derived from the three-band Hubbard model[30] are $t=0.43$ eV, $t'=-0.06$ eV, and $U=4.1$ eV with $\varepsilon=0$ used as reference. These refer to the hole picture. The hopping parameters well represent both electron and hole dynamics in a range of finite clusters. The somewhat larger value of U (5.4 eV) given in Ref. 30 was chosen to most accurately represent the superexchange implied for the insulator by the finite cluster results without concern for simultaneously fitting the charge-transfer gap. The value used here well represents the charge-transfer gap found using the three-band model in the finite clusters. This is important for the present problem. We also note that the resulting superexchange energy is only about 30% larger with the present $U=4.1$ eV. The charge-transfer gap has been calculated for a series of clusters with periodic boundary conditions using the present one-Hubbard model. The result is $\Delta=2.7$ eV, in agreement with the earlier extrapolation from finite cluster calculations[30] but somewhat larger than experiment.[24,51]

Mapping the x-ray-absorption process into this one-band model requires representation of an explicitly O-centered process which is associated to the nearest-neighbor links of Eq. (6). The H_{core} of Eq. (2) must be recast in terms of the parameters in Eq. (6). This is understood as follows. Since no dynamics of the 1s core hole are explicitly considered, only the interaction terms in Eq. (2) need be considered. These enter as a local potential near the core hole in the final-state Hamiltonian. The large U_{cp} centered on a link will disrupt the effective hopping between sites; i.e., it will reduce t for that link. The U_{cd} will act largely as a potential shift ($\Delta\varepsilon$) on the Cu component of the site energy on either side of the link. The U_{cp} will disrupt the singlet formation, while U_{cd}, by effectively reducing $\varepsilon_p-\varepsilon_d$, will enhance the singlet binding. The net resulting change in U for the neighboring sites is a small reduction. The one-band representation of

H_{core} has been explicitly calculated by considering spectra for Cu_2O_7 clusters including a core-hole potential. The resulting local changes are accurately represented by $\Delta\varepsilon_{L(R)}=1.1$ eV, $t_{LR}=0.20$ eV, and $U_{L(R)}=3.7$ eV, where L (R) refers to sites to the left (right) of the link upon which the core hole is created. The value of t' as well as the value of t for other links are not significantly altered. The transition operator appearing in Eq. (3) must be recast in terms of the effective sites. Qualitatively, the link-centered transition must have nonzero amplitude on the underlying O p orbital at the center of the link. With the positive sign for t, the two effective sites must have opposite phase. The effective site has O p character, which varies between the singly and doubly occupied cases. Therefore, we replace $c_{p\sigma}$ in Eq. (3) by

$$\hat{O}_\sigma=\frac{1}{\sqrt{2}}[c_{L\sigma}f(n_L)-c_{R\sigma}f(n_R)]\ . \tag{7}$$

The operator $f(n)$ [Eq. (15)] takes on different values depending on occupancy: $f_1\equiv f(n=1)=0.27$ and $f_2\equiv f(n=2)=0.47$. These were obtained from the calculated XAS for the Cu_2O_7 cluster using the three-band model.

We tested this mapping by explicit comparison with results from the three-band Hubbard model for four Cu-site clusters. This is shown in Fig. 4 for a Cu_4O_{12} cluster with a square geometry and open boundary conditions. The corresponding effective one-band model consists of four sites. As can be seen, the effective one-band model accurately reproduces the calculated absorption cross section both for the insulator (zero extra holes) as well as the hole doped cases. The positions of the main peaks agree to within about 0.2 eV. The peak weights are also accurately reproduced. The upper peak is systematically smaller in the one-band model. However, if we take the scale from the lower peak intensity in the one excess hole case (i.e., "25% doping"), the difference is about 10% or less. This provides one source of uncertainty in the calculated peak intensities presented below. Overall, the agreement is excellent.

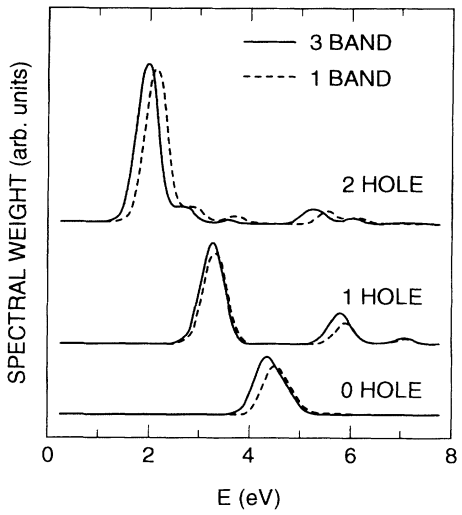

FIG. 4. Comparison of the XAS spectra of Cu_4O_{12} calculated using the extended three-band Hubbard model to the spectra calculated using the one-band Hubbard model for a four-site cluster. Spectra for zero, one, and two extra holes are shown.

The key element of this mapping is to recognize that physical processes which have some chemical specificity must be represented in the one-band model using effective operators that reflect the underlying orbital character of the wave function on the effective side.

B. Model for carrier-concentration fluctuations

The carrier-concentration dependence of the XAS is explicitly considered for the case of $La_{2-x}Sr_xCuO_4$, where the carriers are introduced through Sr doping. Each Sr site has a corresponding "impurity potential" which should be considered in any calculation of spectra. In general terms, one expects at low doping levels to observe the effects of a set of impurity levels in the gap. The precise nature and role of such impurity levels is not clear. In one scenario, the insulator-metal transition occurs in $La_{2-x}Sr_xCuO_4$ at about $x\approx 0.06$.[52] This suggests deeply bound acceptor states with effective radii of order one to two lattice spacings. Model calculations support this picture.[53] In this case, the influence of a strong impurity potential on the XAS must be considered. We have analyzed this in detail, as summarized in the Appendix. The relevant conclusion is that the position and intensities of the peaks are essentially unchanged, once one averages over all distinct O positions relative to the Sr site. This is quite different from the case of photoemission or optical spectra, where states in the gap are directly observable. This result follows from the locality of the x-ray-absorption probe and the chemical shift of the 1s levels by the impurity potential. However, an important consequence of this scenario is that fluctuations in the Sr distribution correspond to fluctuations in local carrier density, at least below the insulator-metal transition. Even in the metal, there will be approximately the same number of carriers locally as Sr atoms to maintain charge neutrality. This again leads to fluctuations in the local carrier density.

An alternative scenario is suggested by transport measurements.[54,55] Analysis of the temperature dependence in the low doping range (O doped but equivalent to $x\approx 0.01$) lead to an activation energy <0.1 eV. This suggests a much weaker perturbation by the impurity potential which may be ignored, given the energy resolution of the XAS. But local fluctuations in carrier density can still be of importance. Consider a simple metal with carrier density x. For a fixed volume, the number of carriers in that volume will be subject to quantum-mechanical fluctuations: $\langle n\rangle=x$ but $\langle(n-x)^2\rangle\neq 0$.

Either scenario leads to the same general conclusion: a certain average doping, e.g., 10%, is *not* the same as the corresponding fixed number of carriers in a small simulation cell, e.g., one carrier in ten sites. There will always be fluctuations in the number of carriers in a cell of fixed size. We argue that a good representation of the spectra for average concentration x is given by an incoherent average:

$$A(\omega,x)=\sum_{n=0}^{N} P_n(x,N)A_n(\omega) . \quad (8)$$

The probability P_n for n carriers in a box of size N sites given average concentration x enters as well as the corresponding spectra for a fixed number of carriers, A_n. The distribution P_n must sum to unity and yield average n equal x. A basic assumption here is that the box size is sufficiently large to contain the physically important correlations for the x-ray-absorption process, within the energy resolution of interest.

In the dilute limit, with a strong impurity potential, there is no coherence between the regions near a dopant (hence with a carrier) and regions without a dopant. Assuming the simulation cell is large enough to enclose the acceptor, the incoherent average of Eq. (8) is appropriate. The Sr dopants are assumed to be randomly distributed without site correlations. Then the probability for the occurrence of n carriers in the simulation cell is the same as for Sr dopants within the equivalent chemical cell. The distribution function derives from Poisson statistics for the occurrence of a Sr atom in a region of N Cu sites for $La_{2-x}Sr_xCuO_4$:

$$P_n(x,N)=\frac{(2N)!}{n!\,(2N-n)!}\left[\frac{x}{2}\right]^n\left[1-\frac{x}{2}\right]^{2N-n} . \quad (9)$$

The factors of 2 in the available sites follow since there are two La atoms per Cu atom. This "impurity" distribution is plotted in Fig. 5 for $x=0.2$ and $N=10$ (open circles).

We emphasize that this argument cannot describe the region near the insulator-metal transition in detail. In the metallic regime, we noted that charge neutrality suggests that the carrier density locally follows the impurity distribution. Therefore the distribution Eq. (9) is still a reasonable choice. Alternatively, quantum-mechanical fluctuations can be modeled by a simple nearest-neighbor tight-binding band for spinless fermions with band occupancy x. This approximates the excess carriers in the Hubbard model. The resulting "metallic" distribution for ten sites with $x=0.2$ is plotted in Fig. 5 (full circles). It is noticeably sharper than the corresponding impurity distribution. In mean-field theory, there are some correlations in the cell occupancy beyond Poisson statistics. Clearly the incoherent average employed in Eq. (8) is a more subtle question. We do note that the length scale for potential (density) fluctuations is comparable to the size of the present simulation cell. Also, the averaging procedure does not alter the coarse graining of the energy spectrum which results from using a finite cell size.

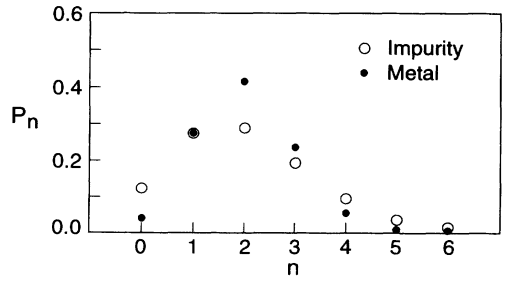

FIG. 5. Probability of n extra holes in a ten-site cluster with average excess hole density of 0.2 calculated from Poisson statistics (open symbol) and a simple (metallic) mean-field model (closed symbol).

For a given simulation cell size, fluctuations near the site of the x-ray-induced transition are taken into account. For sufficiently large cell size, altering the precise number of carriers in the cell would have a negligible impact on the spectrum and the average in Eq. (8) would become irrelevant. We find that the present cell is big enough to contain the important local correlations; the fluctuations accounted for by Eq. (8) are noticeable quantitatively, but do not control the qualitative results.

C. Summary of procedure for calculations

The results presented in the next section are calculated with the one-band Hubbard model described here. The square simulation cell contains ten sites with periodic boundary conditions. Direct diagonalization techniques[38] are used to get the ground state for a given number of holes. For the present parameters, we find that the symmetry of the ground states $(N_\uparrow/N_\downarrow)$ are (5/5) $S=0,\mathbf{k}=\mathbf{0}$; (6/5) $S=\frac{1}{2}$, $\mathbf{k}=\pi(4/5,2/5)$; (6/6) $S=0,\mathbf{k}=\mathbf{0}$ or $\mathbf{k}=\pi(1/5,3/5)$; (7/6) $S=\frac{1}{2},\mathbf{k}=\pi$ (4/5,2/5); and (7/7) $S=0,\mathbf{k}=\mathbf{0}$. The $\mathbf{k}$ vectors are given in units of square lattice parameter $a=1$. The spectral function for the transition operator $\hat{O}_\sigma$ of Eq. (6) is then calculated iteratively applying the Lanczos algorithm to the final-state Hamiltonian, which includes the core-hole potential.[38] The final-state interactions break the translational symmetry in this Hamiltonian. The results are summed over spin configurations of the final state including the core hole. For ground states of nonzero total momentum, spectra must be averaged over symmetry distinct pairs of sites, i.e., a horizontal and a vertical link. Sum rules have been checked, and the spectra presented exhaust more than 99% of the oscillator strength for $\hat{O}$. The spectra for integral excess hole number are then averaged according to Eq. (8) to yield spectra for average carrier density, x.

For comparison to experimental spectra, the calculated spectra are shifted by a common constant which amounts to fixing the otherwise unknown O $1s$ binding energy ε_{1s} in the model Hamiltonian. The relative positions of all the features, as a function of doping, follow directly from the solution of the Hamiltonian without any adjustment. Similarly, the overall amplitude is adjusted only for the insulating case, $x=0$. All other relative intensities derive from the many-body matrix elements without further adjustment.

IV. RESULTS AND DISCUSSION OF EXPERIMENT

In Fig. 6(a), the spectra for fixed carrier number are shown for the ten-site cell. For the insulating case, a single main peak is observed. Physically, the main peak corresponds to transitions into the empty band $(|d^9\rangle\rightarrow|d^{10}\rangle)$, which has an admixture of O p

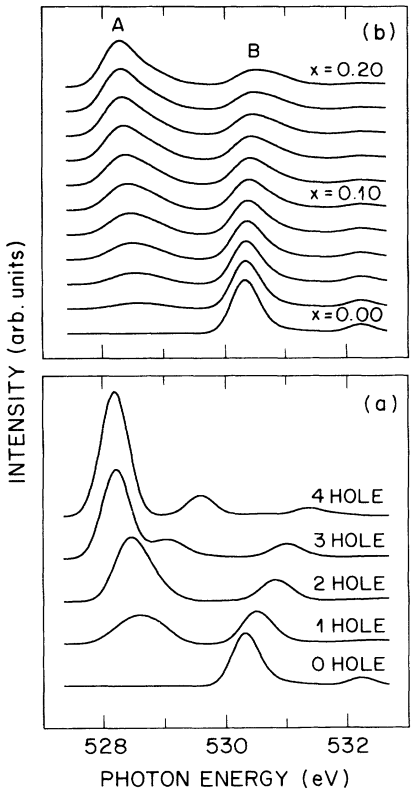

FIG. 6. (a) Calculated O K-edge absorption cross section for the indicated fixed number of excess holes in a planar unit cell containing ten Cu sites. (b) Calculated O K-edge absorption cross section for the indicated range of average excess hole concentrations.

configurations due to hybridization. A small higher-energy feature is also present. It is a remnant of the top of the empty band. (This is clear with reference to Fig. 9.) Upon introduction of excess carriers, a lower-energy peak appears. With increasing number of carriers, the lower peak grows in intensity and shifts to still lower energy. At the same time, the upper peak loses intensity and shifts to higher energy. Physically, the new peak corresponds to transitions into the ligand band ($|d^9\underline{L}\rangle \rightarrow |d^9\rangle$) made possible by the presence of excess holes induced by doping. The separate feature on the high-energy side of the lower peak in the three- and four-hole spectra also appears in the density of states. It is presumably a finite-size effect. The calculated peak separation between the upper peak in the insulator and the lower peak in the one-hole case is about 1.9 eV. This is comparable to, but smaller than, the calculated charge transfer (Mott-Hubbard) gap (2.7 eV). The substantial reduction in the effective gap is due to a core-hole excitonic shift.

The spectra in Fig. 6(a) have been averaged using the "impurity" distribution to yield the absorption cross section as a function of carrier concentration. The results are shown in Fig. 6(b) for $0.0 \leq x \leq 0.2$. This figure provides a smooth visual image for the evolution of the spectra with carrier concentration. The net dispersion of peak A with x is due to the combined effect of motion of the Fermi level and the gain in oscillator strength from the region of peak B. The dispersion of peak B to higher energy reflects the loss of oscillator strength from the low-energy side of the peak. The shape of the peak A is noticeably asymmetric for the present choice of broadening function. This is also a signature of the core-hole excitonic interaction. The increased width of the peaks with larger x is due to the average in Eq. (8).

The spectra in Fig. 6(b) may be analyzed for comparison to experiment. The zeroth, first, and second moments have been calculated for the underlying unbroadened spectra. These moments yield the peak intensity, position, and, when combined with the "experimental" Gaussian FWHM of 0.5 eV, a measure of the peak width, respectively. The analysis of the experimental spectra was presented in Ref. 19. Spectroscopic constants were obtained by fitting to a pair of Gaussians after removal of a common background from each. Deviations from a Gaussian line shape were small.

The comparison between theory and experiment[19] is reproduced in Fig. 7. The rate of growth of peak A together with the corresponding decay of peak B is well reproduced by the theory [Fig. 7(a)]. This transfer of oscillator strength is a key signature in the experiments. The size of the symbols reflects uncertainties in the extraction of the experimental intensities from the data. The "error bar" shown for the theoretical intensity is a best guess for the effect of various sources of uncertainty.

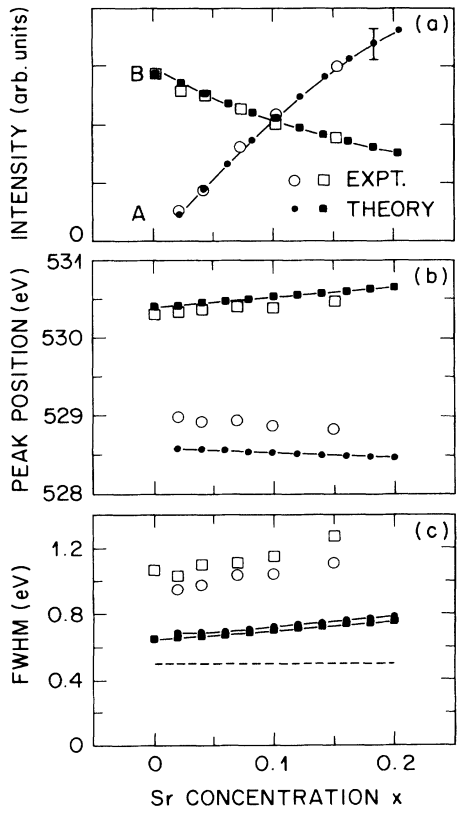

FIG. 7. Comparison of experiment (Ref. 19) and theory for (a) peak intensity, (b) peak position, and (c) peak width of XAS preedge peaks as a function of Sr concentration.

These include the accuracy of the mapping to the one-band model discussed in the preceding section as well as finite-size effects and the choice of distribution function in Eq. (8). The experimental and theoretical peak intensities have been fit by a polynomial in doping concentration, x. Normalizing to the intensity of peak B at $x=0$,

$$M_A = 8.9x - 12.8x^2 \quad \text{(expt.)}, \qquad M_A = 8.6x - 11.5x^2 \quad \text{(theor.)}, \tag{10a}$$

$$M_B = 1.0 - 3.4x + 5.9x^2 \quad \text{(expt.)}, \qquad M_B = 1.0 - 3.3x + 4.3x^2 \quad \text{(theor.)}. \tag{10b}$$

The lower peak A grows in about two to three times faster than the upper peak B decays away. Not only is there transfer of oscillator strength out of peak B, but the total oscillator strength available for XAS is growing rapidly. The latter reflects the predominately O p-character of the states introduced by hole doping. This oscillator strength is discussed in detail in the next section. Overall, the theory accurately reproduces the rate of change of the spectral weights of doping.

The systematic dispersion of the peak positions [Fig. 7(b)] is seen in the calculation. The absolute peak separation is overestimated by about 0.4 eV, mostly because the calculated charge-transfer gap is also too large. Uncertainties in the excitonic shift which traces back to the value calculated for U_{cd} may also contribute. Finally, the calculated width of the peaks [Fig. 7(c)] is seen to be nontrivial. The dashed line shows the width introduced by the line-shape function discussed in Sec. II B. The second moment of the calculated spectral peaks is comparable. The experimental features are substantially broader. There could be several reasons for this. First, the line-shape function was based in part on a value for the O 1s lifetime for a free atom. As noted, it will be shorter in the solid. Second, the results described in the Appendix show that dopant potential effects can lead to a broader lower peak (A). Third, the extraction of a width for peak B in the experimental spectra may be more uncertain because of the background subtraction.

Two sources of uncertainty in the model calculations are analyzed in Fig. 8. The calculated peak intensities for three different distributions P_n are compared in Fig. 8(a): Poisson (impurity) statistics, simple metallic fluctuations, and no average (δ function). They agree by construction for the insulating case (peak B at $x=0$). The systematic trends are independent of the distribution used in averaging. However, the quantitative rate of growth of peak A is slowest for the impurity distribution which is the broadest (Fig. 5). Finite-size effects are empirically assessed in Fig. 8(b). Peak intensities are plotted for eight- and ten-site calculations. The calculation directly yields absorption per O site; no adjustment of scale has been made between the two cases. The upper peak seems to be most sensitive to the boundary conditions. The eight-site cell exhibits first-neighbor coupling within the cell but second-neighbor coupling systematically doubled by the periodic boundary conditions. Boundary effects should be more important for that case. Also, the spectra are noticeably coarser grained. However, peak separation is not significantly altered. Overall, finite-size effects and the details of the averaging do not significantly alter the quantitative results. This suggests that the ten-site cell is sufficiently large to contain the important correlations around the core hole.

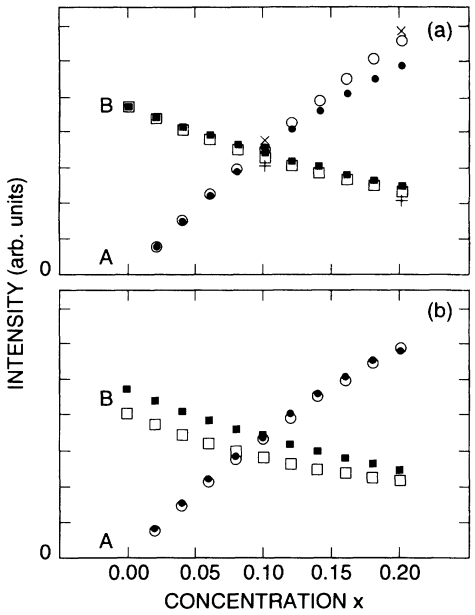

FIG. 8. (a) Comparison of calculated peak intensities as a function of carrier concentration for a Poisson distribution (solid symbols), simple metallic distribution (open symbols), and a δ-function distribution (X, +). (b) Comparison of calculated peak intensities using a Poisson distribution in an eight-site cell (open symbols) and in a ten-site cell (closed symbols).

The Coulomb interaction of the valence holes with the core hole is significant for the shape of the x-ray-absorption spectra. This is illustrated in Fig. 9. The spectra for three carrier concentrations are reproduced by the solid lines. The dashed lines show the corresponding spectra neglecting the effect of the core-hole potential. The two sets of spectra have been aligned at the edge of the lower peak for $x=0.1$. The interaction with the core hole has two striking effects. First, the upper peak is pulled out of the empty band with most of the oscillator strength concentrated in a single peak. The result is a strong peak, shifted down in energy. These attributes probably play an important role in making transitions into the upper Hubbard band observable as a preedge peak in the measured spectrum. This classic core-hole exciton is precisely what occurs in a conventional insulator or semiconductor, e.g., diamond.[56] The band diagram in Fig. 10(a) illustrates how this occurs in the charge-transfer insulator. The local d levels, thought of roughly as a conduction-band edge, are pulled down by U_{cd} adjacent to the core hole. This acts as a potential in the gap, binding down a level. Transitions take place into this empty level below the band edge. Second, the line shape for the lower peak A appearing in the doped material is sharpened towards the Fermi edge. This is due the MND divergence for the simple metal case and traces to the pileup of low-energy electron-hole–pair shakeups. It

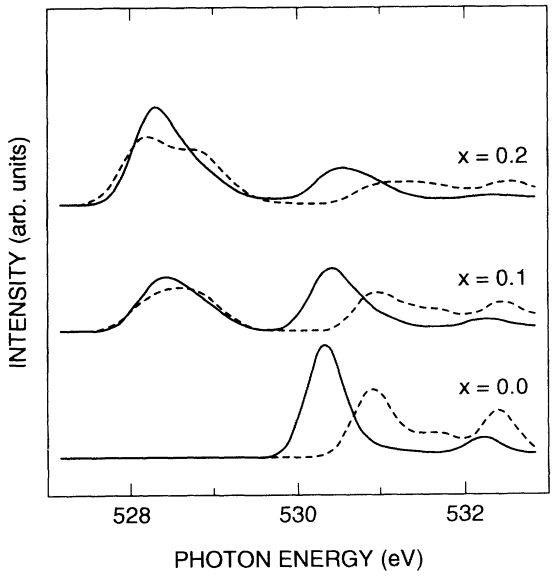

FIG. 9. Calculated XAS spectra for indicated average carrier concentrations with (solid lines) and without (dashed lines) the effect of the core-hole potential, illustrating excitonic effects.

should be noted that this is observed for the present small cell because the density of states is spread out by the strong valence interaction effects. Also, the full effects of the many-body matrix element in Eq. (3) (orthogonality effects) are not developed for such a small number of particles. Finally, if the line shape used in Eq. (3) were broader (e.g., 1 eV), the asymmetry would no longer be evident. The experimental peak A is well fit by the symmetric Gaussian. From this point of view, the lack of asymmetry in the experiment may correspond to the larger width noted in Fig. 7(c).

The observable result of the core-hole potential is summarized in Fig. 10(b) showing that the peak separation is in fact just the charge-transfer gap, reduced by a core-hole exciton binding energy. Frequently, the role of the core-hole exciton has been ignored for the O K edge (e.g., Ref. 13). However, we find that it can be substantial compared to the gap, tracing back to the importance of the first-neighbor core-hole valence Coulomb interaction U_{cd}.

The overall comparison of theory and experiment strongly supports the doped charge-transfer picture of $La_{2-x}Sr_xCuO_4$ well into the metallic regime. This is also consistent with recent EELS measurements.[12] We stress that this insulator derives from strong local correlations in contrast to a conventional ionic insulator. The crucial signature of the correlated band situation is the transfer of oscillator strength in Fig. 7(a).

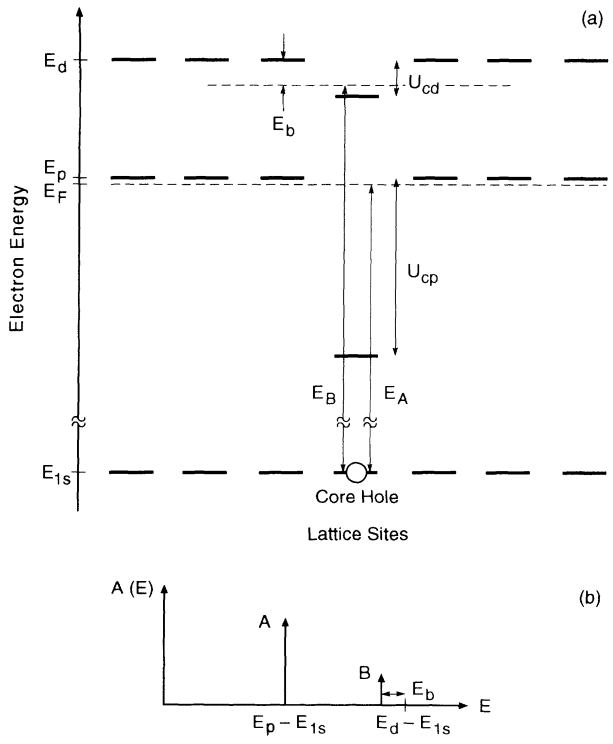

FIG. 10. (a) Band diagram illustrating the role of the core hole Coulomb potential. (b) Schematic spectral function resulting from the band diagram in (a).

V. OSCILLATOR STRENGTH TRANSFER IN A CORRELATED BAND PICTURE

The characteristic decay of peak B in Fig. 1(a) with doping has also been observed for O K-edge spectra from Li-doped NiO.[25] The brief explanation given for this effect relied on earlier arguments applicable to the relative satellite intensities in $L_{2,3}$-edge measurements of NiO.[57] In that case, a final-state destructive interference effect occurs due to the phase between the Ni d and O p orbitals. However, O K-edge spectra calculated for small clusters representing the Cu-O planes of the cuprates show that this particular final-state destructive interference effect occurs only for much-higher-energy final states which are weak and not pertinent here. The final state corresponding to peak B for doped cuprates in fact shows the same phase between the d and p orbitals as that for the lower-energy peak A. Nonetheless, small cluster calculations[58] definitely show the decay in oscillator strength for the upper peak B, as illustrated in Fig. 4. This weight is transferred to the lower peak and derives from a different, more subtle, final-state interference.

In this section, we discuss this characteristic oscillator strength transfer in the context of the one-band Hubbard model. This is a general argument with application to several types of spectra. We first illustrate it for the one-particle Green's function associated with electron addition or removal from a single site in the Hubbard model (IPES or PES). Then, the more complex case of XAS is considered. The key physical features are summarized at the end of the section.

A. Spectral weights: Inverse photoemission

For the single-band model, there is a simple pair of sum rules for the moments of the spectral function below and above the Fermi level, irrespective of correlations:

$$M_i^{\rm pes} \equiv \int_{-\infty}^{E_F} d\omega\, A(\omega) = 2 - \sum_\sigma \langle n_{i\sigma} \rangle = 1 - x \ , \quad (11a)$$

$$M_i^{\rm ipes} \equiv \int_{E_F}^{\infty} d\omega\, A(\omega) = \sum_\sigma \langle n_{i\sigma} \rangle = 1 + x \ . \quad (11b)$$

The spectral function is normalized to give a total of two for the full band. The operator $n_{i\sigma}$ refers to the hole density. The concentration x of excess holes is given by $\sum_\sigma \langle n_{i\sigma} \rangle = 1 + x$. These are exact results. The discussion of transfer of oscillator strength focuses on the spectral distribution of the $1+x$ available empty states, above the Fermi level.

For a simple, uncorrelated ionic insulator, doped with excess holes from a source which only weakly perturbs the lattice potential, the distribution of empty states is trivial. The usual conduction band has weight 1 in the present units independent of carrier concentration while the band opened up by doping has weight x. This situation could be altered by strong potential perturbations leading to impurity levels deep in the gap. These would pull spectral weight from both the valence and the conduction band. However, this would not lead to the present situation of two peaks still separated by approximately the full gap.

The correlated band picture is qualitatively different. We first consider the case of no hopping, i.e., $t = 0$, and make the argument for the one-band Hubbard model in the electron picture. [Referring to Fig. 1(b), the zero of energy is in the ligand band.] In the insulator, the empty band is separated from the occupied band by the Coulomb energy U. When adding an electron to probe empty states, there are N sites on which to place it, with spin opposite to the electron already present, always at energy U. Now consider the hole-doped case with one excess hole. There are still $N-1$ sites where it requires energy U to add the electron. However, on the site of the extra hole, the electron may be added with either spin up or spin down, with zero energy. From this one sees that the higher-energy band has *lost one* contribution, while the lower-energy band has *gained two* contributions for every added hole. For finite excess hole density x, the weight of the upper bands becomes $1-x$, while the lower-energy band induced by doping has weight $2x$. The correlated picture gives a strikingly different spectral distribution of empty states than does the simple ionic band picture. Part of the weight in the band at high energy is transferred to the low-energy region as holes are introduced.

The strong local Coulomb interaction gives a *static* transfer of oscillator strength. When the hoping is restored, the upper and lower bands spread out. For the parameter range appropriate to the cuprates, the Coulomb interaction is strong enough to maintain a (pseudo)gap between the upper band and the band introduced by doping. Quantitatively, the fluctuations introduced by the hopping lead to an additional *dynamic* transfer of oscillator strength which further *enhances* the strength of the low-energy peak at the expense of the higher-energy peak.

Harris and Lange[59] developed a theory of spectrally resolved moments in the limit of small t/U. This analysis provides the integrated weight in each discrete band. However, it does not distinguish between empty and occupied states. When carried out strictly to order t/U in the operators, one finds the weight for the bands at energies zero and U,

$$M_{i;0} = \sum_\sigma \langle n_{i\sigma} \rangle + T_i = 1 + x + T_i \ , \quad (12a)$$

$$M_{i;U} = 2 - \sum_\sigma \langle n_{i\sigma} \rangle - T_i = 1 - x - T_i \ , \quad (12b)$$

which includes the static transfer described above as well as a dynamic transfer of weight between the two spectral regions given by[60]

$$T_i = \frac{1}{U} \sum_{j\sigma} t_{ij} \langle (1 - n_{i-\sigma} - n_{j-\sigma})(c_{i\sigma}^\dagger c_{j\sigma} + c_{j\sigma}^\dagger c_{i\sigma}) \rangle \ . \quad (13)$$

The hopping matrix t_{ij} includes t and t' of Eq. (6). All operators refer to the hole picture. The dynamic transfer is related to the average kinetic energy per site of the extra carriers. The factor involving the density operators serves to project out the kinetic energy associated with superexchange; $T_i \approx 0$, for half filling. Physically, the dynamic transfer for the doped case is due to intersite interference. Near the extra hole, the final state can consist of singly occupied nearest-neighbor sites or a doubly occupied site and an empty site. These channels are coupled by the hopping and constructively (destructively) interfere for the lower (upper) band in the hole-doped case ($T_i > 0$).

We now discuss the moments for the case of IPES. For hole doping, the entire spectral weight at high energy (i.e., $M_{i;U}$) is due to the empty states. This together with the sum rule Eq. (11b) gives the portion of spectral weight at low energy (i.e., $M_{i;0}$) which is above the Fermi level:

$$M_{i;0}^{\rm ipes} = M_i^{\rm ipes} - M_{i;U} = 2x + T_i \ \ \text{(dopant band)} \ , \quad (14a)$$

$$M_{i;U}^{\rm ipes} = M_{i;U} = 1 - x - T_i \ \ \text{(upper band)} \ . \quad (14b)$$

This is a general result. It includes static transfer and an explicit expression for the dynamic transfer T_i in Eq. (13), which is valid to order t/U.

The transfer of oscillator strength is illustrated in Fig. 11(a). The spectral weight function is plotted for a sequence of excess hole numbers in the ten-site lattice for the present parameters in Eq. (6). The transfer of weight from the upper band to the dopant band above the Fermi level is quite evident. Furthermore, one can see that qualitatively the weight is pulled from the near edge of the upper band. The upper band appears to disperse to higher energy while the lower band both expands to lower energy as the Fermi level drops as well as expanding into the gap region. The apparent band-edge separation remains about constant. For the present parameters, at least a pseudogap persists to quite high hole concentrations. (A weak tail may extend through the gap.) However, the spectral strength above the gap is systematically depleted. This effect has also been observed in other calculations, both within the three-band[61,62] as well as the one-band Hubbard model.[62,63]

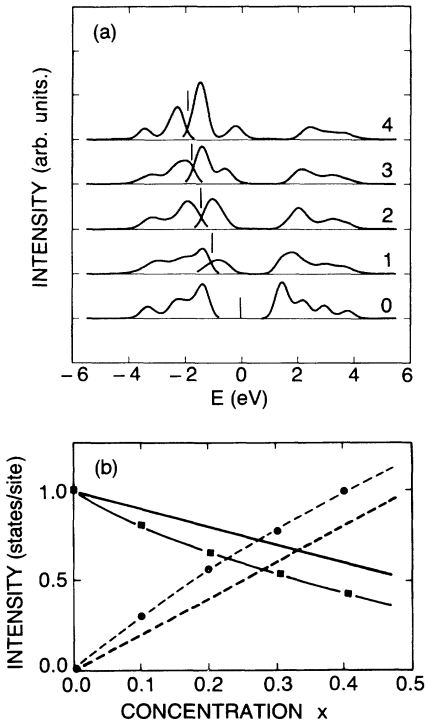

FIG. 11. (a) Hole and electron parts of the imaginary part of the one-particle Green's function for the effective one-band Hubbard model as a function of excess hole count in a ten-site cell (Gaussian broadened, 0.5-eV FWHM). The zero of energy is set to midgap in the insulator and the Fermi energy is indicated by the ticks. (b) Calculated oscillator strength in the upper and lower bands of the empty part of the one-particle Green's function as a function of excess hole concentration (solid symbols, with lines to guide the eye). One unit corresponds to a half filled band in the free-electron case. The lines indicate the static $t/U \to 0$ result $1-x$ and $2x$, respectively.

The calculated spectral strength in the empty portion of each band is plotted in Fig. 11(b). The lines indicate the static oscillator strength. The dynamic transfer is the difference. It is quantitatively important because it is *linear* in t/U, being due to intersite interference. Although $t/U \approx 0.1$ in the present case, T_i is nonnegligible. Numerical evaluation of Eq. (13) shows that the t/U expansion yields much of the dynamical transfer in Fig. 11(b) (e.g., 70% for $x=0.2$).

B. Spectral weights: X-ray absorption

X-ray absorption near the O K edge is more complicated than IPES and contains interesting new features. Since a link-centered operator is used, cross terms arise in the various expressions for the moments with new interference effects. This is reasonable since the O p valence enters the one-band Hubbard model in part dynamically through the hopping integrals. There are also final-state effects due to the core hole which influence the spectral distribution. However, explicit calculation shows that the transfer of weight from peak B to peak A is enhanced by no more than about 10% due to the core-hole potential. For simplicity, we do not include the core-hole potential in the subsequent discussion and focus on the qualitatively larger effects due to the form of the transition operator.

The transition operator, Eq. (7), can be written out explicitly as

$$\hat{O}_{ij\sigma}=\frac{1}{\sqrt{2}}\{f_i[c_{i\sigma}(1-n_{i-\sigma})-c_{j\sigma}(1-n_{j-\sigma})] + f_2(c_{i\sigma}n_{i-\sigma}-c_{j\sigma}n_{j-\sigma})\}\ , \tag{15}$$

where the density operators explicitly project singly and doubly occupied sites. The ij are the pair of sites that define the link (the O site) and hence are always nearest-neighbor pairs. The zeroth moments of the spectral function for $\hat{O}_{ij\sigma}$ give the total weight in emission and absorption, the analog of the sum rules in Eqs. (11):

$$M_{ij}^{\rm emis}=f_2^2-f_2^2x-M_{ij}^d-M_{ij}^t, \tag{16a}$$

$$M_{ij}^{\rm abs}=f_1^2+(2f_2^2-f_1^2)x+M_{ij}^d+M_{ij}^t\ . \tag{16b}$$

Two contributions alter the moments:

$$M_{ij}^d=\tfrac{1}{2}(f_2^2-f_1^2)\sum_\sigma\langle(n_{i\sigma}-1)(n_{i\sigma}-1) + (n_{j\sigma}-1)(n_{j-\sigma}-1)\rangle\ , \tag{17a}$$

$$M_{ij}^t=-\tfrac{1}{2}\sum_\sigma\langle[f_1^2+2f_1(f_2-f_1)n_{i-\sigma} + (f_2-f_1)^2n_{i-\sigma}n_{j-\sigma}] \times(c_{i\sigma}^\dagger c_{j\sigma}+c_{j\sigma}^\dagger c_{i\sigma})\rangle\ . \tag{17b}$$

There are two important differences from Eqs. (11): (i) the factors f_1 and f_2 distinguish the O valence for singly and doubly occupied sites; (ii) the moments explicitly include dynamic terms. Physically, $M^{\rm abs}$ has enhanced weight due to the static O p valence of doubly occupied sites introduced by hole doping, $(f_2^2-f_1^2)x$. The dynamic terms are M_{ij}^d, which measures fluctuations creating an extra doubly occupied site and an empty site, and M_{ij}^t, which derives explicitly from the hopping. Both contribute to the effective O valence, although M_{ij}^d is small, being effectively higher order in t/U. The total spectral weight *depends* on the doping concentration:

$$M_{ij}^{\rm abs}+M_{ij}^{\rm emis}=(f_1^2+f_2^2)+(f_2^2-f_1^2)x\ . \tag{18}$$

This traces to the dependence of the static O valence on the local occupancy in the one-band Hubbard model. This varies with doping. The total number of real O p states is constant. However, only part of the p manifold is actually represented in the one-band model. The fraction covered depends on doping.

The spectrally resolved weights for $\hat{O}_{ij\sigma}$ may be calculated to order t/U:

$$M_{ij;0}=f_2^2(1+x)+T_{ij}\ , \tag{19a}$$

$$M_{ij;U}=f_1^2(1-x)-T_{ij}\ . \tag{19b}$$

The transfer contains a diagonal term as in the preceding section plus a cross term:

$$T_{ij}=\tfrac{1}{2}f_1f_2(T_i+T_j)-f_1f_2T_{ij}^c \ , \tag{20}$$

where T_i is given in Eq. (13) and the cross term is

$$T_{ij}^c=\frac{t_{ij}}{U}\sum_\sigma \langle (c_{j\sigma}^\dagger c_{i\sigma}c_{j-\sigma}^\dagger c_{i-\sigma}+\text{c.c.}) + [n_{i-\sigma}+n_{j-\sigma}-2n_{i-\sigma}n_{j-\sigma} + (c_{j\sigma}^\dagger c_{i\sigma}c_{i-\sigma}^\dagger c_{j-\sigma}+\text{c.c.})]\rangle \ . \tag{21}$$

The first term represents a correlated double hop between sites i and j, which requires one to be doubly occupied while the other is empty. This is a small contribution, being higher order in t/U when evaluated. The second term acts together on pairs of sites which have one spin on each site, projecting out singlet combinations. It is a measure of short-range antiferromagnetic order. For a pair of sites with an extra hole, only the density operators act, either constructively or destructively, with T_i+T_j depending on the relative phase for the extra hole on sites i and j. When evaluated for the hole-doped case, both $T_i>0$ and $T_{ij}^c>0$, so there are competing effects in T_{ij}. The weight in the individual x-ray-absorption peaks is obtained by combining Eqs. (19b) and (16b):

$$M_{ij;0}^{\text{abs}}=M_{ij}^{\text{abs}}-M_{ij;U}=2f_2^2x+T_{ij}+M_{ij}^d+M_{ij}^t \quad (\text{peak } A) \ , \tag{22a}$$

$$M_{ij;U}^{\text{abs}}=M_{ij;U}=f_1^2(1-x)-T_{ij} \quad (\text{peak } B) \ . \tag{22b}$$

This is a general result with the expressions for T_{ij} correct to order t/U. The static transfer is enhanced by the extra O valence assigned to a doubly occupied site. For the case of the insulator ($x=0$), $T_{ij}=-(M_{ij}^d+M_{ij}^t)$ to first order in t/U.

The total spectral weight in the absorption spectrum is shown in Fig. 12(a) for zero, one, and two extra holes in the ten-site cluster (no statistical averaging). For comparison to IPES, the spectral weights are given in units of states per site. For the insulator, the value of about 0.2 states/site is essentially the O p weight in the ground state, as calculated earlier in the three-band model.[30] This rises rapidly with doping since added holes have predominately O p character. The solid line gives the static contribution from Eq. (16b). The dynamic contributions from M_{ij}^d and M_{ij}^t, represented by the difference, are significant even for the insulator. They grow slowly with doping. The individual peak weights are plotted in Fig. 12(b). Results from Sec. IV (without core-hole potential) are indicated by the solid symbols. The open symbols show the results of the first-order expressions Eqs. (19). The order t/U results well represent the full calculations. The errors are indicated by the nonzero spectral weight for peak A in the insulator (about 5% of peak B) which result from combining the exact expressions Eqs. (16) with the first-order results to get Eqs. (22). The first-order expression for T_{ij} deviates from $-(M_{ij}^d+M_t)$ by about 20% for $x=0$.

The decay of peak B consists of two parts. First, there is the static transfer of oscillator strength discussed previously. The solid line shows the contribution, which is the first term in Eq. (22b), plus the dynamic contribution to the O P valence in the insulator $T_{ij}(x=0)$. The static transfer accounts for 30–40% of the loss in spectral weight. Second there is the change in the dynamic transfer. T_{ij} is also shown in Fig. 12(b). This is the other 60–70% of the loss in peak B. The change in T_{ij} is about half due to decay of local antiferromagnetic spin correlations measured by the second term in Eq. (21). The other half is derived from the mechanism discussed for inverse photoemission (T_i). The static contribution to the growth of peak A is shown by the dashed line in Fig. 12(b). It accounts for about 60–70% of the weight. The dynamic contributions to the O p valence together with transfer from peak B account for the remaining 30–40%.

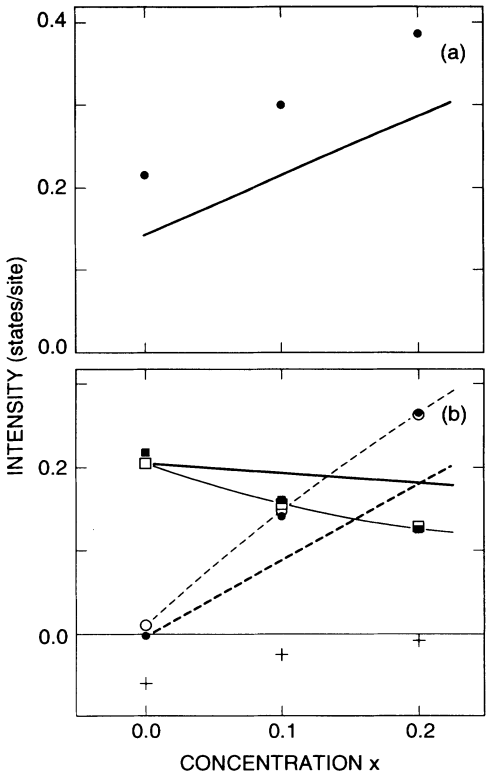

FIG. 12. (a) Calculated total intensity in the x-ray-absorption cross section in units of states per site (solid symbols) as a function of hole concentration. Solid line gives the static contribution. (b) Weights in peak A and peak B separately from the full calculation (solid symbols, without effects of the core-hole potential) in comparison to the first-order expressions Eqs. (22) (open symbols, with lines to guide the eye). Dashed and solid lines from the static term and the dynamic transfer term T_{ij} are plotted separately (+).

This gives a detailed account of the spectral weight transfer implied by the present one-band Hubbard model for x-ray absorption near the O K edge. Although the numerical results are for modest size clusters, the expressions are general and the trends are established. Equations (22) could be used more generally with a comparable order approximation for evaluating the necessary expectation values.[64]

An interesting question to ask is whether the XAS places constraints on the strength of the local interactions, i.e., the value of U/t in the one-band Hubbard model. Using the general expressions discussed above, we have analyzed the calculated moments as a function of U/t. For each value, f_1 can be regarded as a disposable parameter which can be fit to give the rate of growth of the total absorption, M^{abs}. The value of f_2 is fixed since it reflects the fact that doubly occupied sites are approximately 50% O p and 50% Cu d in general. Based on this analysis, we conclude that the rates of change of the XAS peak intensities roughly constrain U/t to the range 8–10. Larger values would lead to the contradictory result that the O p valence in the insulator (f_1) should be an *increasing* function of U/t (essentially the charge-transfer gap). Substantially smaller values of U/t cannot be analyzed using the t/U expansions used here. However, for a value of U/t smaller than 6, the gap between the preedge peaks in the XAS for the metallic samples would collapse. For the present value of t, U/t less than about 8 would lead to a charge-transfer gap smaller than experiment.

C. Summary of peak intensity evolution with doping

The systematic dependence of the spectral weight on doping concentration is one of the key signatures in the x-ray-absorption experiment. We have given a detailed, general analysis of the spectral weights within the one-band Hubbard model. The O p valence is probed by the O K-edge measurements. The strength of peak B in the insulator is proportional to the p valence admixed in the insulator. The holes added by doping are predominately O p character. Therefore, the new transitions which give peak A in the doped material are proportionately stronger. In the one-band Hubbard model, these effects are manifested both through static and dynamic contributions, but this is the physical explanation. The strong local Coulomb interactions lead to a static transfer of weight from peak B to peak A as extra holes are introduced by doping, enhanced by the extra p valence associated with the dopant holes. There is an additional dynamic transfer which derives from final-state intersite interference and the reduction of local antiferromagnetic correlations upon doping. This transfer of oscillator strength is responsible for the decay of peak B with doping and contributes to the rate of growth of peak A.

In comparing with the rigid density of states depicted in Fig. 1(b), the striking feature of the data is the decay of the intensity of peak B. We have shown that the correlated band picture, exemplified by the present Hubbard model, naturally explains that behavior. These results should extend beyond the restricted range of the present one-band model. For example, the results in the Appendix show that the spectral weight distribution for x-ray absorption is *not* disrupted by a strong impurity potential which could be associated with the doping process. This is despite the fact that the corresponding level is quite deep and would dramatically alter the one-particle Green's function. We also expect that longer-range Coulomb interactions will not qualitatively change the spectral distribution, provided that the corresponding valence exciton binding energy is not too large compared with the optical gap.

VI. DISCUSSION OF RELATED EXPERIMENTS

Photoemission and IPES can probe the states near the Fermi level. Two widely cited results appear to contradict the XAS data and our interpretation in terms of a doped charge-transfer insulator. First, the Fermi level appears to be pinned during doping with new states filling in the gap region,[6] in contrast to Fig. 1. Second, the Fermi surface area mapped out by angle-resolved PES is "large" in agreement with band theory.[43] This is to be contrasted with the naive picture, implied by a doped insulator model, of "pockets" with area proportional to the doping density. We discuss both points and conclude with comparisons to optical data.

Direct comparison of PES from $La_{2-x}Sr_xCuO_4$ and $Nd_{2-x}Ce_xCuO_4$ suggested that the Fermi level was pinned at the same position independent of whether it was n or p doped.[6] This alignment was inferred because the main valence-band feature in the photoemission spectra (near -3 eV) was at the same relative binding energy for both materials. The weakness with this argument is the differences in crystal structure of the two materials, with corresponding differences in electronic structure. Detailed evidence for this comes from band-structure calculations which should give reliable estimates for crystal-field and hybridization differences. The calculated Fermi level is about 1.2–1.4 eV from the first prominent edge in the valence-band density of states in La_2CuO_{45}.[29] However, in Nd_2CuO_4, the separation is only about 0.2–0.4 eV.[65] This suggests that there could be as much as a 1-eV difference between the materials in the position of the Fermi level relative to the ligand p-band side of the charge-transfer gap. In other words, the apparent constant distance between the Fermi level and the main valence-band feature could be due to a cancellation of two shifts of order 1 eV. A different type of experiment has been done actually monitoring the change in the Fermi level with further addition of holes to an existing metallic system. Upon adding further O to $Bi_2Sr_2CaCu_2O_{8+\delta}$, motion of the Fermi level deeper into the band by about 0.2 eV is observed, consistent with a conventional doping picture.[66] Finally, recent x-ray PES data have been obtained for Y counterdoped samples, which allows study of the motion of the Fermi level from the metallic regime back to the insulator. Several core levels as well as the main valence-band peak were monitored showing substantial Fermi-level shifts, also consistent with a conventional doping picture.[67]

If the Fermi level were pinned near midgap independent of doping, an alternative bandlike scenario might be proposed.[6] The states induced by doping would fill in the gap drawing weight equally from both sides of the charge-transfer gap to recover the continuous density of states found in the band calculations. The data from photoemission do *not* uniformly support such a scenario. The predictions of the one-band Hubbard model with the

present parameters (but *no* impurity potential) were illustrated in Fig. 11 and contradict this scenario. The Fermi level moves from somewhere in the gap for the insulator into the band upon doping, in agreement with other, similar calculations.[63] The XAS neither confirms nor contradicts such changes in chemical potential directly since only one type of carrier was introduced. However, the data in Fig. 1(a) do support the robustness of the underlying bulk charge-transfer gap as well as subsequent motion of the Fermi level into the band with further doping. The present work therefore suggests that the charge-transfer gap derived features do not collapse upon doping.

The states near the Fermi level have been extensively mapped out for $YBa_2Cu_3O_{6.9}$ using angle-resolved PES.[43] The results show a large area Fermi surface which is in remarkably close agreement with band calculations. Similar agreement has been obtained for $Bi_2Sr_2CaCu_2O_8$.[68] This might appear to contradict the model of a doped charge-transfer insulator. Operationally, the Fermi surface separates regions of high and low momentum density, i.e., $n(\mathbf{k})>\frac{1}{2}$ vs $n(\mathbf{k})<\frac{1}{2}$, where $n(\mathbf{k})=\langle c^{\dagger}_{\mathbf{k}\sigma}c_{k\sigma}\rangle$. In the calculations for the one-band Hubbard model, or equivalently the *t-J* model, the Fermi surface defined in this way has been found to have a volume corresponding to all the particles in the band, not just the extra carriers.[69,70] The local spins contribute actively, beyond forming the background medium. Arguments based on the resonating valence-bond ground state for the doped Hubbard model[44] have also suggested that transport coefficients such as the Hall number would be proportional to doping while the apparent Fermi surface would correspond to all the spins.[71,72] The parameters used for the *t-J* model calculations of the Fermi surface in Ref. 70 are compatible with those used here and derived earlier.[30] Thus, the one-band Hubbard model used here to describe the XAS is apparently consistent with the large Fermi surface observed for other cuprates.

There are several interesting comparisons to optical measurements. The measured peak separation in XAS (1.3 eV initially) is similar to the onset of the charge-transfer band measured optically [1.8 eV (Ref. 24)]. The optical transition is in principle shifted by a valence exciton binding energy. Both gaps have the same physical origin, but with quantitatively different excitonic shifts. The calculated 0.8-eV excitonic shift in the XAS would then be consistent with a 0.3–0.4-eV valence exciton binding energy. However, measured photocurrent spectra give a threshold for charge-transfer excitations of 2.0 ± 0.1 eV.[55] This suggests a somewhat smaller valence exciton binding energy of ≈ 0.2 eV. The rapid buildup of low-energy oscillator strength in the optical spectra upon doping[37] is accompanied by a collapse of intensity at the charge-transfer energy.[24] This is similar to the transfer of spectral weight found in XAS and may have a similar explanation. However, further work is required to explore this suggestion. Finally, impurity-induced levels, while not important for XAS, may play an important role in the distribution of low-energy transitions observed optically.[73] Deep impurity levels would influence only the low-energy side of peak *A* in the XAS (see the Appendix). They do not fill in the observed peak separation, a point of confusion in the literature.[12,13]

VII. CONCLUSIONS

The detailed, quantitative analysis of the x-ray-absorption spectra of $La_{2-x}Sr_xCuO_4$ presented in this paper has relied heavily on our earlier work deriving parameters for a three-band Hubbard model to represent La_2CuO_4 (Ref. 28) and our mapping of these results onto a one-band Hubbard model.[30] Here we find that a chemically specific spectroscopic probe (i.e., XAS) for states near the charge-transfer gap can be well represented by an effective one-band Hubbard model with definite parameters and a clear physical interpretation of the operators. The favorable comparison between theory and experiment should be regarded as strong support for essential features of that one-band Hubbard model. Perhaps it is more useful to turn the argument around. The x-ray-absorption spectra reflect three essential aspects of the electronic structure: (i) the O *p* valence as a function of doping: (ii) the size of the charge-transfer gap; and (iii) the strength of the coupling (U/t). The analysis in Sec. V clearly supports the importance of local correlations and the adequacy of the one-band Hubbard model to represent these three essential features. The observed rate of change of the spectral weights with doping seems to require a value of U/t in the range 8–10 together with the approximate O *p* valence used here (20–30 % *p* character in the insulator and 70–80 % *p* character for holes added by doping). This is clearly in the range where strong local correlation effects are important. It does not exclude the possibly important role of impurity potentials, further neighbor Coulomb interactions, or other interactions for explaining other properties of the cuprates. However, it does add support to our basic framework for describing the electronic structure.

In summary, we have presented strong evidence that the electronic structure of the cuprates can be well described as a doped charge-transfer insulator well into the metallic (superconducting) regime. This model explains the XAS in detail. It is compatible with many other data, including the observed area of the Fermi surface. It remains a challenge to understand the implications of this model in detail for experiments which probe the electronic structure of the cuprates on a smaller energy scale.

ACKNOWLEDGMENTS

It is a pleasure to acknowledge close collaboration with experimental colleagues at AT&T Bell Laboratories who performed the measurements summarized by Fig. 1 and presented in Ref. 19. We thank Professor B. Chakraborty for bringing Ref. 59 to our attention. One of us (E.B.S) gratefully acknowledges useful discussions with Dr. D. R. Jennison. Work done at Sandia National Laboratories was supported by the U.S. DOE under Contract No. DE-AC04-76DP00789.

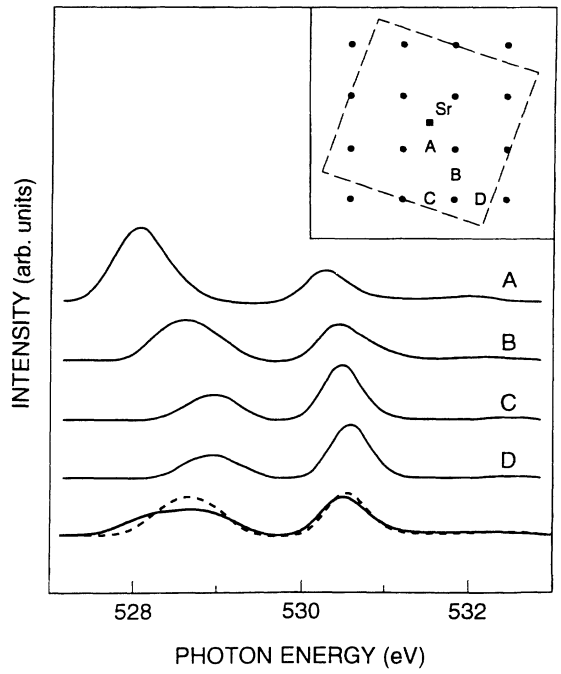

FIG. 13. XAS spectra with one extra hole for O atoms at four different sites relative to a Sr impurity atom calculated in the effective one-band Hubbard model. The final curves show the spectrum averaged over O sites (solid line) in comparison to the spectrum calculated in the abscence of the dopant potential (dashed line). The inset shows the cluster geometry and the O sites ($A-D$).

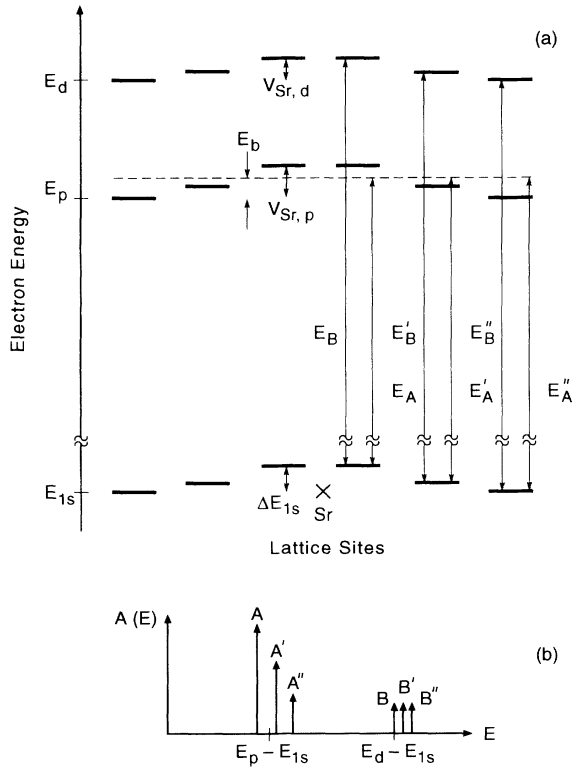

FIG. 14. (a) Band diagram illustrating the role of the dopant potential due to a Sr impurity atom. (b) Schematic spectral function resulting from the band diagram.

APPENDIX: EFFECT OF STRONG IMPURITY POTENTIALS

Following earlier work,[52] the Sr acceptor potential is modeled by that of a statistically screened ($\varepsilon \approx 5$) point charge centered at the Sr site. In the one-band Hubbard model, the first shell potential shift is $V_{\text{imp},1} = -0.89$ eV, the second-neighbor shell is $V_{\text{imp},2} = -0.46$ eV, etc. Calculations were done in a ten-site cell with periodic boundary conditions. The ground-state calculations with, and without, the dopant hole in the presence of the impurity potential establish an acceptor binding energy of 0.7 eV. About 75% of the acceptor hole charge density is localized on the first-neighbor shell of four sites. The spectra for all the symmetry distinct O sites (links) in the simulation cell must be averaged to obtain the cross section per O site. There are four distinct O sites (labeled $A-D$) shown in the inset to Fig. 13. The acceptor potential also introduces a chemical shift of the O 1s core levels, which is used to align the spectra for sites $A-D$.

X-ray transitions, which occur near the dopant where the acceptor hole charge density is large, should show an intense lower preedge peak. Far from the dopant, the spectrum should recover to the insulator with a single preedge peak. In Fig. 13, the lower preedge peak is intense for site A and decays with distance while shifting to higher energy as the sites get further from the dopant. The upper preedge peak is weak for site A, but recovers intensity with a small shift. The average spectrum is very similar to the spectrum for an extra hole in the absence of the dopant potential. The lower peak is inhomogeneously broadened by the deep acceptor.

These results can be understood in simple terms. Figure 14(a) is a real-space presentation of the on-site energies in the presence of the dopant potential. By analogy to a band diagram for a doped semiconductor, the gap region is between the p level and the d level with most of the available empty states above this "conduction-band edge." The dopant potential locally shifts the p and d levels as well as the O 1s core level. The p levels are locally pushed into the gap region creating an attractive potential well for excess holes which binds the deep acceptor level (dashed line) by E_b. This level is the new empty state introduced by doping. For transitions from each O 1s level, the electron may be placed into the acceptor level from site i giving a component of peak A:

$$E_{A,i} = E_p - E_{1s} + E_b - \Delta E_{1s,i} \ .$$

The amplitude for this transition is proportional to the acceptor envelope function, decaying quickly to zero outside the radius of the acceptor. The electron may also be placed into the conduction band, as in the insulator. However, since these are local transitions, they probe the local density of states which will peak near the local d level contributing to peak B:

$$E_{B,i} \approx E_d - E_{1s} + V_{sr,d,i} - \Delta E_{1s,i} \ .$$

The d- and 1s-level shifts are approximately the same, so the transition energy B is only slightly perturbed from its value in the insulator.

The combined transitions for sites at varying distances from the Sr dopant give a spectrum sketched in Fig. 14(b). Transitions into the acceptor level are strongest near the Sr site, decaying further away. The shift in position is due to the combined effect of the constant acceptor binding energy E_b and the spatially varying chemical shift of the 1*s* level. This implies that the signature of the acceptor levels occurs on the *low-energy side* of the lower-energy preedge peak *A*. The separation between peak *A* and *B* is *not reduced* by the deep accelerator level.

---

*Present address: Physics Department, Blackett Laboratory, Imperial College, London.

[1]A. Fujimori, E. Takayama-Muromachi, Y. Uchida, and B. Okai, Phys. Rev. B **35**, 8814 (1987).

[2]Z.-X. Shen, J. W. Allen, J. J. Yeh, J.-S. Kang, W. Ellis, W. Spicer, I. Lindau, M. B. Maple, Y. D. Dalichaouch, M. S. Torikachvili, J. Z. Sun, and T. H. Geballe, Phys. Rev. B **36**, 8414 (1987).

[3]J. C. Fuggle, P. J. W. Weijs, R. Schoorl, G. A. Sawatzky, J. Fink, N. Nucker, P. J. Durham, and W. M. Temmerman, Phys. Rev. B **37**, 123 (1988).

[4]D. van der Marel, J. van Elp, G. A. Sawatzky, and D. Heitmann, Phys. Rev. B **37**, 5136 (1988).

[5]A. J. Arko, R. S. List, R. J. Bartlett, S.-W. Cheong, Z. Fisk, J. D. Thompson, C. G. Olson, A.-B. Yang, R. Liu, C. Gu, B. W. Veal, J. Z. Liu, A. P. Paulikas, K. Vandervoort, H. Claus, J. C. Campuzano, J. E. Schriber, and N. D. Shinn, Phys. Rev. B **40**, 2268 (1989).

[6]J. W. Allen, C. G. Olson, M. B. Maple, J.-S. Kang, L. Z. Liu, J.-H. Park, R. O. Anderson, W. P. Ellis, J. T. Markert, Y. Dalichaouch, and R. Liu, Phys. Rev. Lett. **64**, 595 (1990).

[7]J. A. Yarmoff, D. R. Clark, W. Drube, U. O. Karlsson, A. Taleb-Ibrahimi, and F. J. Himpsel, Phys. Rev. B **36**, 3967 (1987).

[8]N. Nucker, J. Fink, B. Reker, D. Ewert, C. Politis, P. J. W. Weijs, and J. C. Fuggle, Z. Phys. B **67**, 9 (1987).

[9]N. Nucker, J. Fink, J. C. Fuggle, P. J. Durham, and W. M. Temmerman, Phys. Rev. B **37**, 5158 (1988).

[10]N. Nucker, H. Romberg, X. X. Xi, J. Fink, B. Gegenheimer, and Z. X. Zhao, Phys. Rev. B **39**, 6619 (1989).

[11]H. Romberg, N. Nucker, M. Alexander, J. Fink, D. Hahn, T. Zetterer, H. H. Otto, and K. F. Renk, Phys. Rev. B **41**, 2609 (1990).

[12]H. Romberg, M. Alexander, N. Nucker, P. Adelmann, and J. Fink, Phys. Rev. B **42**, 8768 (1990).

[13]M. Alexander, H. Romberg, N. Nucker, P. Adelmann, J. Fink, J. T. Markert, M. B. Maple, S. Uchida, H. Takagi, Y. Tokura, A. C. W. P. James, and D. W. Murphy, Phys. Rev. B **43**, 333 (1991).

[14]P. Kuiper, G. Kruizinga, J. Ghijsen, M. Grioni, P. J. W. Weijs, F. M. F. de Groot, G. A. Sawatzky, H. Verweij, L. F. Feiner, and H. Petersen, Phys. Rev. B **38**, 6483 (1988).

[15]F. J. Himpsel, G. V. Chandrasekhar, A. B. McLean, and M. W. Shafer, Phys. Rev. B **38**, 11 946 (1988).

[16]E. E. Alp, J. C. Campuzano, G. Jennings, J. Guo, D. E. Ellis, L. Beaulaigue, S. Mini, M. Faiz, Y. Zhou, B. W. Veal, and J. Z. Liu, Phys. Rev. B **40**, 9385 (1989).

[17]A. Krol, C. S. Lin, Z. H. Ming, C. J. Sher, Y. H. Kao, C. T. Chen, F. Sette, Y. Ma, G. C. Smith, Y. Z. Zhu, and D. T. Shaw, Phys. Rev. B **42**, 2635 (1990).

[18]A. Krol, C. S. Lin, Z. H. Ming, C. J. Sher, Y. H. Kao, C. L. Lin, S. L. Qiu, J. Che, J. M. Tranquada, M. Strongin, G. C. Smith, Y. K. Tao, R. L. Meng, P. H. Hor, C. W. Chu, G. Cao, and J. E. Crow, Phys. Rev. B **42**, 4763 (1990).

[19]C. T. Chen, F. Sette, Y. Ma, M. S. Hybertsen, E. B. Stechel, W. M. C. Foulkes, M. Schluter, S.-W. Cheong, A. S. Cooper, L. W. Rupp, Jr., B. Batlogg, Y. L. Soo, Z. H. Ming, A. Krol, and Y. H. Kao, Phys. Rev. Lett. **66**, 104 (1991).

[20]J. Zaanen, G. A. Sawatzky, and J. W. Allen, Phys. Rev. Lett. **55**, 418 (1985).

[21]P. Nozieres and C. T. De Dominicis, Phys. Rev. **178**, 1097 (1969).

[22]G. D. Mahan, Phys. Rev. **163**, 612 (1967).

[23]P. W. Anderson, Phys. Rev. Lett. **18**, 1049 (1967).

[24]J. Orenstein, G. A. Thomas, D. H. Rapkine, C. G. Bethea, B. F. Levine, B. Batlogg, R. J. Cava, D. W. Johnston, Jr., and E. A. Rietman, Phys. Rev. B **36**, 8892 (1987); S. Tajima, S. Tanaka, T. Ido, and S. Uchida, J. Opt. Soc. Am. **6**, 475 (1989).

[25]P. Kuiper, G. Kruizinga, J. Ghijsen, G. A. Sawatzky, and H. Verweig, Phys. Rev. Lett. **62**, 221 (1989).

[26]V. J. Emery, Phys. Rev. Lett. **58**, 3759 (1987); C. M. Varma, S. Schmitt-Rink, and E. Abrahams, Solid State Commun. **62**, 681 (1987).

[27]A systematic study has suggested that the small admixture of $d(3z^2-r^2)$ and $p(z)$ varies with material according to T_c: A. Bianconi, P. Castrucci, A. Fabrizi, M. Pompa, A. M. Flank, P. Lagarde, H. Katayoma-Yoshida, and G. Calestani, in *Earlier and Recent Aspects of Superconductivity,* edited by J. G. Bednorz and K. A. Muller (Springer-Verlag, Berlin, 1990), p. 407. However, more recent studies find a much smaller admixture: S. Suziki, T. Takahashi, T. Kusunoki, T. Morikawa, S. Sato, H. Katayama-Yoshida, A. Yamanaka, F. Minami, and S. Takekawa, Phys. Rev. B **44**, 5381 (1991).

[28]M. S. Hybertsen, M. Schluter, and N. E. Christensen, Phys. Rev. B **39**, 9028 (1989).

[29]L. F. Mattheiss, Phys. Rev. Lett. **58**, 1028 (1987); J. Yu, A. J. Freeman, and J.-H. Xu, *ibid.* **58**, 1035 (1987).

[30]M. S. Hybertsen, E. B. Stechel, M. Schluter, and D. R. Jennison, Phys. Rev. B **41**, 11 068 (1990).

[31]E. B. Stechel and D. R. Jennison, Phys. Rev. B **38**, 4632 (1988).

[32]A. K. McMahan, R. M. Martin, and S. Satpathy, Phys. Rev. B **38**, 6650 (1989); A. K. McMahan, J. F. Annett, and R. M. Martin, *ibid.* **42**, 6268 (1990); J. B. Grant and A. K. McMahan, Phys. Rev. Lett. **66**, 488 (1991).

[33]J. Zaanen, O. Jepsen, O. Gunnarsson, A. T. Paxton, and O. K. Andersen, Physica C **153-155**, 1636 (1988).

[34]F. Mila, Phys. Rev. B **38**, 11 358 (1988).

[35]H. Eskes, L. H. Tjeng, and G. A. Sawatzky, Phys. Rev. B **41**, 288 (1990).

[36]E. B. Stechel, M. S. Hybertsen, and M. Schluter (unpublished).

[37]S. L. Cooper, G. A. Thomas, D. H. Rapkine, A. J. Millis, S.-W. Cheong, D. Rytz, A. S. Cooper, and Z. Fisk, Phys. Rev. B **41**, 11 605 (1990).

[38]R. Haydock, in *Solid State Physics,* edited by F. Seitz and D. Turnbull (Academic, New York, 1980), Vol. 35, p. 216; J. K. Cullum and R. A. Willoughby, *Lanczos Algorithms for Large Symmetric Eigenvalue Computations* (Birkhauser, Cambridge,

1985).
[39]F. Sette, C. K. Wertheim, Y. Ma, G. Meigs, S. Modesti, and C. T. Chen, Phys. Rev. B **41**, 9766 (1990).
[40]O. K. Andersen, Phys. Rev. B **12**, 3060 (1975); H. L. Skriver, *The LMTO Method* (Springer-Verlag, New York, 1984).
[41]M. Grioni, M. T. Czyzyk, F. M. F. De Groot, J. C. Fuggle, and B. E. Watts, Phys. Rev. B **39**, 4886 (1989).
[42]J. Zaanen, M. Alouani, and O. Jepsen, Phys. Rev. B **40**, 837 (1989).
[43]J. C. Campuzano, G. Jennings, M. Faiz, L. Beaulaigue, B. W. Veal, J. Z. Liu, A. P. Paulikas, K. Vandervoort, H. Claus, R. S. List, A. J. Arko, and R. J. Bartlett, Phys. Rev. Lett. **64**, 2308 (1990).
[44]P. W. Anderson, Science **235**, 1196 (1987).
[45]F. C. Zhang and T. M. Rice, Phys. Rev. B **37**, 3759 (1988).
[46]H. Eskes, G. A. Sawatzky, and L. F. Feiner, Physica C **160**, 424 (1989).
[47]C.-X. Chen, H.-B. Schuttler, and A. J. Fedro, Phys. Rev. B **41**, 2581 (1990); H.-B. Schuttler and A. J. Fedro (unpublished).
[48]J. F. Annett and R. M. Martin, Phys. Rev. B **42**, 3929 (1990).
[49]H. Eskes and G. A. Sawatzky, Phys. Rev. B **44**, 9656 (1991).
[50]S. B. Bacci, E. R. Gagliano, R. M. Martin, and J. F. Annett, Phys. Rev. B **44**, 7504 (1991).
[51]J. Humlicek, M. Garriga, and M. Cardona, Solid State Commun. **67**, 589 (1988).
[52]J. B. Torrance, Y. Tokura, A. I. Nazzal, A. Bezinge, T. C. Huang, and S. S. P. Parkin, Phys. Rev. Lett. **61**, 1127 (1988).
[53]K. Rabe and R. Bhatt, J. Appl. Phys. **69**, 4508 (1991).
[54]N. W. Preyer, R. J. Birgeneau, C. Y. Chen, D. R. Gabbe, H. P. Jenssen, M. A. Kastner, P. J. Picone, and T. Thio, Phys. Rev. B **39**, 11 563 (1989).
[55]T. Thio, R. J. Birgeneau, A. Cassanho, and M. A. Kastner, Phys. Rev. B **42**, 10 800 (1990).
[56]J. F. Morar, F. J. Himpsel, G. Hollinnger, G. Hughes, and J. L. Jordan, Phys. Rev. Lett. **54**, 1960 (1985). The observed exciton is not the lowest-energy bound exciton due to matrix element effects: K. A. Jackson and M. R. Pederson, Phys. Rev. Lett. **67**, 2521 (1991).
[57]C. van der Laan, J. Zaanen, G. A. Sawatzky, R. Karnatak, and J.-M. Esteva, Phys. Rev. B **33**, 4253 (1986).
[58]H. Eskes and G. A. Sawatzky, Phys. Rev. B **43**, 119 (1991).
[59]A. B. Harris and R. V. Lange, Phys. Rev. B **157**, 295 (1967).
[60]Equation (13) includes an extra density factor which does not appear in Eqs. (5.20) of Ref. 59. Numerical tests of Eq. (13) for the ten-site cluster suggest it yields the correct order t/U contribution to the oscillator strength transfer.
[61]P. Horsch, W. H. Stephan, K. v. Szczpanski, M. Ziegler, and W. von der Linden, Physica C **162-164**, 783 (1989).
[62]H. Eskes, M. B. J. Miendes, and G. A. Sawatzky, Phys. Rev. Lett. **67**, 1035 (1991).
[63]E. Dagotto, A. Moreo, F. Ortolani, J. Riera, and D. J. Scalapino, Phys. Rev. Lett. **67**, 1918 (1991).
[64]E. B. Stechel and M. S. Hybertsen (unpublished).
[65]S. Massidda, N. Hamada, J. Yu, and A. J. Freeman, Physica C **157**, 571 (1989).
[66]Z.-X. Shen, D. S. Dessau, B. O. Wells, C. G. Olson, D. B. Mitzi, L. Lambado, R. S. List, and A. J. Arko, Phys. Rev. B **44**, 12 098 (1991).
[67]R. Itti, F. Munakata, K. Ikeda, H. Yamauchi, N. Koshizuka, and S. Tanaka, Phys. Rev. B **43**, 6249 (1991); M. van Veenendaal, R. Schlatmann, W. A. Groen, and G. A. Sawatzky (unpublished).
[68]C. G. Olson, R. Liu, D. W. Lynch, R. S. List, A. J. Arko, B. W. Veal, Y. C. Chang, P. Z. Jiang, and A. P. Paulikas, Phys. Rev. B **42**, 381 (1990).
[69]A. Moreo, D. J. Scalapino, R. L. Sugar, S. R. White, and N. E. Bickers, Phys. Rev. B **41**, 2313 (1990).
[70]W. Stephan and P. Horsch, Phys. Rev. Lett. **66**, 2258 (1991).
[71]P. W. Anderson, Phys. Rev. Lett. **64**, 1839 (1990).
[72]N. Nagaosa and P. Lee, Phys. Rev. Lett. **64**, 2450 (1990).
[73]G. A. Thomas, D. H. Rapkine, S. L. Cooper, S.-W. Cheong, A. S. Cooper, L. F. Schneemeyer, and J. V. Waszczak, Phys. Rev. B **45**, 2474 (1992).

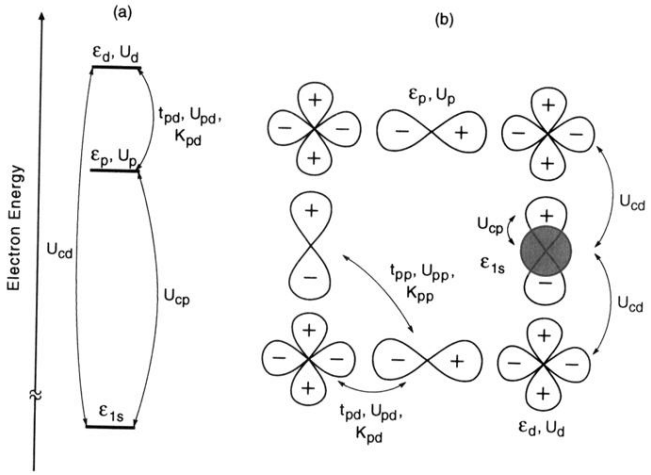

FIG. 2. Illustration of the extended three-band Hubbard model showing all the interactions including those involving the O 1*s* core level. (a) The level structure shown for electron energies. (b) The orbitals retained in the CuO_2 planes.